High-resolution Neural Network Demonstrates Strong CO2 Source-Sink Juxtaposition in the Coastal Zone

Patrick J. Duke[1], Roberta C Hamme[1], Debby Ianson[2], Peter Landschützer[3], Neil C. Swart[4], and Paul Covert[5]

[1]University of Victoria
[2]Institute of Ocean Sciences
[3]Flanders Marine Institute
[4]Environment Canada
[5]Institute of Ocean Sciences, Fisheries and Oceans Canada

March 21, 2024

Abstract

Coastal oceans may play an important role in regulating the concentration of carbon dioxide in the atmosphere. Quantification of carbon fluxes at this highly dynamic land-ocean interface will aid in monitoring, reporting, and verification for marine carbon dioxide removal. Here, we use a two-step neural network approach to generate basin-wide estimates from sparse observational data in the coastal Northeast Pacific Ocean at an unprecedented spatial resolution of 1/12° with coverage in the nearshore (0 - 25 km offshore). We compiled partial pressure of carbon dioxide (pCO2) observations as well as a range of predictor variables including satellite-based and physical oceanographic reanalysis products. With the predictor variables representing processes affecting pCO2, we created non-linear relationships to interpolate observations from 1998-2019. Compared to in situ shipboard and mooring observations, our coastal pCO2 product captures broad spatial patterns and seasonal cycle variability well. A sensitivity analysis identifies that the parameters responsible for the neural network's ability to capture regional pCO2 variability agrees with mechanistic processes. Using wind speed and atmospheric CO2, we calculated air-sea CO2 fluxes. We report an anticorrelation between net annual air-sea CO2 flux and air-sea CO2 flux seasonal amplitude and suggest the relationship is driven by regional processes. We show the inclusion of nearshore net outgassing fluxes lowers the overall regional net flux. Overall, our results suggest that the region is a net sink (-0.7 mol m-2 yr-1) for atmospheric CO2 with trends indicating increasing oceanic uptake due to strong connectivity to subsurface waters.

Hosted file

`Duke_AGU_2024.docx` available at https://authorea.com/users/757644/articles/730328-high-resolution-neural-network-demonstrates-strong-co2-source-sink-juxtaposition-in-the-coastal-zone

Hosted file

`Duke_AGU_2024_SuppInfo.docx` available at https://authorea.com/users/757644/articles/730328-high-resolution-neural-network-demonstrates-strong-co2-source-sink-juxtaposition-in-the-coastal-zone

High-resolution Neural Network Demonstrates Strong CO_2 Source-Sink Juxtaposition in the Coastal Zone

P. J. Duke[1], R. C. Hamme[1], D. Ianson[1,2], P. Landschützer[3], N. C. Swart[1,4], P. A. Covert[2]

[1]School of Earth and Ocean Sciences, University of Victoria, Victoria, BC, Canada

[2]Institute of Ocean Sciences, Fisheries and Oceans Canada, Sidney, BC, Canada

[3]Flanders Marine Institute (VLIZ), Ostend, Belgium

[4]Canadian Centre for Climate Modelling and Analysis, Environment and Climate Change Canada, Victoria, BC, Canada

Corresponding author: P. J. Duke (pjduke@ucalgary.ca)

Key Points:

- The coastal Northeast Pacific is a net sink for atmospheric CO_2 with increasing air-sea pCO_2 disequilibrium trends in most of the region.
- Regional processes drive net annual air-sea CO_2 flux to be anticorrelated with air-sea CO_2 flux seasonal amplitude.
- Estimated pCO_2 reproduces observed seasonal cycle phase and amplitude well along with broad spatial patterns of variability.

Abstract

Coastal oceans may play an important role in regulating the concentration of carbon dioxide in the atmosphere. Quantification of carbon fluxes at this highly dynamic land-ocean interface will aid in monitoring, reporting, and verification for marine carbon dioxide removal. Here, we use a two-step neural network approach to generate basin-wide estimates from sparse observational data in the coastal Northeast Pacific Ocean at an unprecedented spatial resolution of 1/12° with coverage in the nearshore (0 - 25 km offshore). We compiled partial pressure of carbon dioxide (pCO_2) observations as well as a range of predictor variables including satellite-based and physical oceanographic reanalysis products. With the predictor variables representing processes affecting pCO_2, we created non-linear relationships to interpolate observations from 1998-2019. Compared to *in situ* shipboard and mooring observations, our coastal pCO_2 product captures broad spatial patterns and seasonal cycle variability well. A sensitivity analysis identifies that the parameters responsible for the neural network's ability to capture regional pCO_2 variability agrees with mechanistic processes. Using wind speed and atmospheric CO_2, we calculated air-sea CO_2 fluxes. We report an anticorrelation between net annual air-sea CO_2 flux and air-sea CO_2 flux seasonal amplitude and suggest the relationship is driven by regional processes. We show the inclusion of nearshore net outgassing fluxes lowers the overall regional net flux. Overall, our results suggest that the region is a net sink (-0.7 mol m^{-2} yr^{-1}) for atmospheric CO_2 with trends indicating increasing oceanic uptake due to strong connectivity to subsurface waters.

Plain Language Summary

The importance of the coastal ocean as a hub of exchange for carbon between terrestrial ecosystems, the open ocean, and the atmosphere is still unclear. In this study, we investigate how much carbon dioxide moves between the ocean and the atmosphere in the coastal Northeast Pacific. We use a mathematical technique (i.e., machine learning) to transform limited observational data to a high-resolution estimate of this exchange across the entire region. We found this method effectively captured the big picture patterns and seasonal changes in ocean carbon dioxide levels. We report that the coastal Northeast Pacific absorbs slightly more carbon dioxide than it releases, helping regulate atmospheric levels of this greenhouse gas. However, there are large differences regionally with some coastal zones absorbing substantial amounts of carbon dioxide and others releasing the gas, such as the nearshore. We report a trend of increasing ocean uptake over time, suggesting the region may play an increasingly important role

in reducing atmospheric carbon dioxide levels. This study provides valuable baseline information for efforts to reduce carbon dioxide in the atmosphere through artificially enhancing ocean uptake in the region.

1 Introduction

The global ocean takes up nearly a quarter of anthropogenic carbon dioxide (CO_2) emissions annually (Friedlingstein et al., 2023). It has been suggested coastal oceans contribute disproportionately to oceanic CO_2 uptake relative to global ocean by surface area (Bourgeois et al., 2016; Chau et al., 2022; Laruelle et al., 2014; Resplandy et al., 2024; Roobaert et al., 2019, 2024), but exhibit far greater heterogeneity in air-sea CO_2 fluxes (Liu et al., 2010) and may be changing at a different rate compared to the open ocean (Laruelle et al., 2018; Resplandy et al., 2024). Coastal oceans serve as an important hub of exchange, outgassing carbon delivered by terrestrial ecosystems to the ocean (Regnier et al., 2022), while facilitating transport between the coast and open ocean, and directly absorbing CO_2 from the atmosphere (Bauer et al., 2013; C.-T. A. Chen & Borges, 2009; Mackenzie et al., 1998; Ward et al., 2020). However, the role of the coastal ocean in the global carbon budget is not well-constrained due to lack of observations relative to the complexity of highly localized variability (Chavez et al., 2007; Dai, 2021; Dai et al., 2022).

Gap filling approaches (i.e., methods to interpolate sparse observations) used to inform coastal ocean air-sea CO_2 flux estimates are often at coarse resolution and often operate as a "black box." Interpolation techniques have been widely used to inform air-sea CO_2 flux estimates in the coastal ocean both regionally and globally (e.g., S. Chen et al., 2016; Hales et al., 2012; Laruelle et al., 2017; G. Parard et al., 2015; Gaëlle Parard et al., 2016; Roobaert et al., 2019, 2024; Sharp et al., 2022; Xu et al., 2019). These approaches extend the temporal and spatial coverage of partial pressure of CO_2 in seawater (pCO_2) observations from community synthesis efforts (e.g., through the Surface Ocean CO_2 Atlas (SOCAT); Bakker et al., 2016) and can be used to calculate air-sea CO_2 fluxes using wind speed and atmospheric CO_2 (Wanninkhof, 2014). Historically, coastal ocean approaches have been adopted from their open ocean counterparts (Chau et al., 2022; Landschützer, Laruelle, et al., 2020), and thus most of these estimates have at best a monthly, 1/4°x1/4° latitude by longitude resolution, which is incapable of resolving smaller scale processes in coastal regions, especially nearshore, that experience high variability and short autocorrelation length scales (Jones et al., 2012). Interpolation techniques, which lack transparency, also rarely probe internal relationship dependency between variables.

Large heterogeneity in air-sea CO_2 fluxes exist in the coastal Northeast Pacific, with substantial expanses of the coast completely absent of observations (Benway et al., 2016). Large discrepancies exist between previous air-sea CO_2 flux estimates within this region, with disagreement over the net annual flux magnitude and direction (i.e., as a net sink or source for atmospheric CO_2; Duke, Richaud, et al., 2023; Fennel et al., 2019). Air-sea CO_2 flux variability in the region is heavily impacted by coastal processes such as upwelling, river plumes, tidal mixing, and coastal currents (Evans et al., 2012, 2019; Evans & Mathis, 2013; Hales et al., 2005; Ianson et al., 2003; Nemcek et al., 2008). Upwelling along the Pacific eastern boundary shelf has contrasting impacts on the oceanic CO_2 sink reflected in complex interactions between biological carbon drawdown fueled by upwelled nutrient and carbon-rich waters (Hales et al., 2005; Messié & Chavez, 2015; Ribalet et al., 2010) and outgassing associated with the same subsurface waters brought to the surface (Chan et al., 2017; Christensen, 1994; Evans et al., 2011; Feely et al., 2008; Hales et al., 2005; Ianson & Allen, 2002). Closer to shore, within the Salish Sea, and along Alaska's Inside Passage, air-sea CO_2 fluxes into and out of the ocean are highly episodic and spatially heterogeneous (Evans et al., 2022; Jarníková, Ianson, et al., 2022). Binning regional pCO_2 observations in three dimensions into monthly, 1/12°x1/12° grid cells over the period 1998–2019, reveals the data scarcity (Figure 1). Of the 6,030,816 spatial and temporal grid cells just 0.6% have an associated gridded pCO_2 value. Observations are concentrated along shipping lanes, have a summer bias, and increase in frequency during later years (Figure 1). No observations exist in vast areas of the coastal Gulf of Alaska and along extensive stretches of shoreline (Figure 1c).

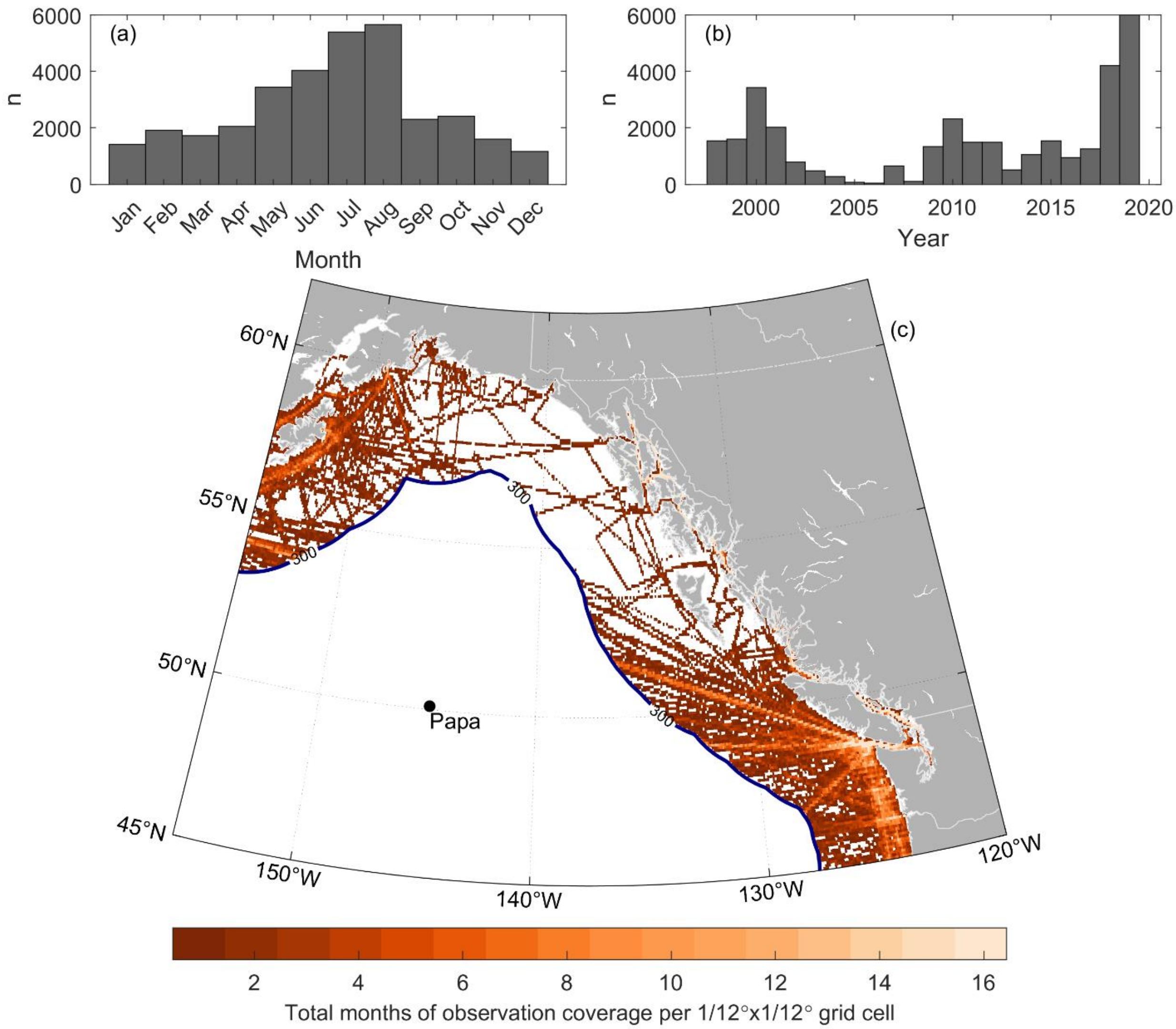

Figure 1. Number of grid cells (of 54782 total spatial grid cells) with coastal $p\mathrm{CO_2}$ observation data (Section 2.1) in (a) months reveals a summer bias, and (b) years showing increased sampling closer to present. (c) Total number of months of observational coverage per grid cell displays better coverage along shipping routes. 300 km offshore line shown for coastal/open oceanic boundary used in this study (solid blue line labelled '300').

Here we investigate how well a high-resolution regional artificial neural network (ANN) approach can determine air-sea CO_2 fluxes in the coastal Northeast Pacific (NEPc). We build on an existing global setup (Landschützer et al., 2013) adopted previously in stepping to a higher spatial resolution in the open Northeast Pacific (Duke, Hamme, et al., 2023b). In Section 2, we describe the creation of a gridded $p\mathrm{CO_2}$ data product for the coastal Northeast Pacific monthly from January 1998 to December 2019 at an unprecedented 1/12°x1/12° resolution to resolve coastal ocean processes. In Section 3, we demonstrate that our product robustly recreates gridded observation data, comparable to a less variable open ocean product. In Section 4, we directly compare our pCO_2 product with *in situ* shipboard and mooring observations and detail potential capabilities and limitations in the continuous, gridded product. In Section 5, we examine the regional patterns of variability in the net annual air-sea CO_2 flux relative to the seasonal cycle and describe potential drivers through a spatial sensitivity analysis. We conclude by calculating surface ocean pCO_2 trends in the last decades.

2 Data and methods

We created a coastal pCO_2 data product spanning a geographic area between 45 - 62°N and 120 - 155°W, and within 6 to 300 km of shore building on the methods of Duke, Hamme, et al. (2023b). (ANN-NEPc; Duke et al., 2024). Briefly, our first step identified grid cells with similar environmental characteristics, provinces, using a self-organizing map approach (SOM) (Landschützer et al., 2013). In the second step, within each province, we used a feed-forward neural network (FFN) to create non-linear functional relationships between pCO_2 observations and independent predictor variables (Landschützer et al., 2013). Third, we applied these relationships to the predictor data to generate continuous monthly sea surface pCO_2 maps from 1998-2019 in the coastal Northeast Pacific (NEPc). ANN-NEPc fills the gap between open ocean (> 300 km offshore) pCO_2 (Duke, Hamme, et al., 2023b) to as close to the shoreline as reanalysis and satellite-based products reach. In stepping to 1/12° spatial resolution (approximately 9 km by 5 km, latitude by longitude), this work represents a three times increase in spatial resolution over previous 1/4° global and regional coastal ocean products with an overlapping domain (Landschützer, Laruelle, et al., 2020; Laruelle et al., 2017; Roobaert et al., 2024; Sharp et al., 2022), with extended coverage into the nearshore (defined here as 0 - 25 km offshore).

2.1 pCO_2 observations

ANN target pCO_2 data came from the Surface Ocean CO_2 Atlas (SOCAT) v2021 (Bakker et al., 2016), the Fisheries and Oceans Canada February 2019 Line P cruise (https://www.waterproperties.ca/linep/), a West Coast Ocean Acidification cruise from July and August 2010 (Evans et al., 2012), and La Perouse cruises from May 2007 and May 2010 (Tortell et al., 2012). Sea surface CO_2 fugacity (fCO_2) was converted to sea surface pCO_2 (supplementary Text S1; Körtzinger, 1999). We did not correct *in situ* pCO_2 observations to sea surface mass boundary layer temperature, because following previous techniques introduced significant additional uncertainty in our coastal study area (supplementary Text S2). pCO$_2$ observations were bin-averaged (monthly from 1998–2019, at 1/12°x1/12°), computing the mean and standard deviation within each grid cell.

2.2 Predictor data

Predictor data were chosen based on accessibility and ability to represent processes that mechanistically impact surface ocean pCO$_2$ (Table 1). Selected predictor variables primarily originate from satellite observations or reanalysis models (Table 1; supplementary Text S3). Predictors differ slightly from a regional open ocean estimate (Duke, Hamme, et al., 2023b). Here, we used a high-resolution regional wind speed product and not reanalysis model derived mixed layer depth. Capturing greater variability in the coastal ocean required a high-resolution regional wind speed product over a low-resolution global product (supplementary Figure S2). Latitude, longitude, and time were not used as predictor variables.

Table 1. Northeast Pacific Coastal Ocean artificial neural network predictor variables, and their corresponding source, original temporal and spatial resolutions, and processing steps used for this study.

Predictor variable	Source	Original resolution		Processing
		Temporal	Spatial	
Satellite-based product				
Sea surface temperature (SST)	SST_cci: Level 4 Analysis Climate Data Record, version 2.1	Daily	1/20°x1/20°	Averaged to monthly, aggregated to 1/12°x1/12°
Chlorophyll-*a* (Chl)	Ocean_Colour_cci: Version 5.0	Daily	1/24°x1/24°	Averaged to monthly, aggregated to 1/12°x1/12°, log10-transformed
Satellite and in-situ observation data assimilated reanalysis product				
Sea surface salinity (SSS)	Copernicus Marine Service GLOBAL_REANALYSIS_PHY_001_030	Monthly	1/12°x1/12°	None
Sea surface height (SSH)				None
Atmospheric-measurement-based interpolation product				
Atmospheric pCO_2	Landschützer et al. (2020b) - NCEI Accession 0160558	Monthly	1°x1°	Interpolated to 1/12°x1/12°
High-resolution regional forecast model				
Wind speed	Regional Deterministic Reforecast System (RDRS-v2.1)	Hourly	1/11°x1/11°	Averaged to monthly, interpolated to 1/12°x1/12°

2.3 Neural network construction

To reach the optimal ANN-NEPc architecture, we performed a series of tuning tests using the MATLAB Neural Network Toolbox, with sequential improvements impacting future tests (Duke, Hamme, et al., 2023b). The choice of three dynamic (i.e., changing shape at every timestep) self-organizing map (SOM) based clusters represented the lowest number for a typical clustering structure to emerge (supplementary Figure S3a). All spatial grid cells within the study area belong to more than one SOM cluster at some point over 1998-2019 (supplementary Figure S3b). SOM predictor variables (SST, SSS, SSH only; Table 1) were normalized to a mean of 0 and standard deviation of 1. The second FFN step used all six predictor variables in Table 1, in addition to each predictor variable anomaly (i.e., deseasonalized; calculated by subtracting the climatological monthly mean), bringing the total number of predictors to 12. Anomaly values were used to highlight interannual to decadal variability within our predictor data sets. The number of neurons within the first hidden layer varied by province with the optimal number of neurons determined in a pre-training run (Landschützer et al., 2013, 2014). The second hidden layer used seven static neurons, which slightly improved performance. To further decrease the risk of overfitting, we used a 10-fold cross-evaluation approach to create an ANN ensemble (Duke, Hamme, et al., 2023b; Li et al., 2019, 2020) and a bootstrapping method (Landschützer et al., 2013). Observation cruises were randomly divided into 10 equal subsamples (10% each) using expocodes (i.e., unique identifiers corresponding to complete underway cruise tracks or mooring deployments) prior to gridding, leaving some data splits with more (or less) gridded $p\mathrm{CO_2}$ targets (Section 2.1). We repeated the FFN training step 10 times, using each of the 10 subsamples once as the internally withheld evaluation dataset and the rest as the training dataset (with a separate independent data always withheld; Section 2.4). In each iteration, we trained the ANN for 10 rounds. The robustness and reliability of an ANN estimate has been shown to be significantly improved by combining a ANN ensemble (Duke, Hamme, et al., 2023b; Fourrier et al., 2020; Linares-Rodriguez et al., 2013; Sharkey, 1999). Here, we take the mean of the 10-fold estimates.

2.4 Evaluation

Comparisons of ANN output to training and independent withheld data were made throughout tuning tests. ANN-NEPc performance for each tuning test was evaluated using five statistical metrics: root mean squared error (RMSE), coefficient of determination (r^2), mean absolute error (MAE), mean bias (calculated as the mean residual), and the slope of the linear regression (c_1) between the ANN and the corresponding gridded $p\mathrm{CO_2}$ observations. One subset of data was selected from the observation data using associated expocodes to be entirely withheld from the FFN training step. We tested 100 random independent withheld data splits and selected the one with the best observational coverage over a wide range of seasons, years, and locations (supplementary Figure S4). These independent withheld data represented approximately 4.5% of the total study area gridded $p\mathrm{CO_2}$ data.

2.5 Sensitivity analysis

We used a perturbation approach to quantitatively assess the impact of each predictor variable on estimated $p\mathrm{CO_2}$ (e.g., Broullón et al., 2018; Li et al., 2020; Sun et al., 2021). To diagnose how important different predictor variables were across the study area, a single set of non-linear relationships was used inside a single uniform SOM cluster. We then applied this single FFN to our continuous, gridded predictor dataset and to perturbed versions of that dataset. For each predictor variable separately, we introduced a perturbation increasing the value within each grid cell by 50% of the standard deviation within that grid cell ($X' = X + 0.5(std(X))$; N = 264 months per grid cell; de Oña & Garrido, 2014) and calculated the resulting predicted pCO_2. We then took the difference between the perturbed run and a baseline run using unperturbed predictor variables.

2.6 Computation of air-sea fluxes

Using our pCO_2 product, we calculated the air-sea CO_2 flux ($F\mathrm{CO_2}$; mol m^{-2} yr^{-1}):

$$F\mathrm{CO_2} = K_0 k \Delta p\mathrm{CO_2}\,, \tag{1}$$

from the Henry's Law solubility constant (K_0; mmol m^{-3} μatm^{-1}) as a function of temperature and salinity (Table 1; Weiss, 1974), gas transfer velocity (k; m day^{-1}), and the gradient between pCO_2 in the surface ocean and the atmosphere (ΔpCO_2; μatm). Here, the gas transfer velocity is derived from Wanninkhof (2014), a function of wind-speed at 10 meter elevation (Table 1) and the temperature dependent Schmidt number specific to CO_2 (Wanninkhof, 2014). Negative flux values indicate CO_2 uptake by the ocean. We assume that the uncertainty in our air-sea CO_2 flux estimate results from a 20% uncertainty in k (Wanninkhof, 2014) and the overall product uncertainty in estimated pCO_2 (θpCO_2; Section 3.3 below). As the uncertainty of ΔpCO_2 is dominated by the uncertainty in estimated surface ocean pCO_2, we neglect the small contribution from atmospheric CO_2 (< 1 μatm; Landschützer et al., 2014).

3 Network performance

3.1 Evaluation with respect to observational data

Comparing our estimated pCO_2 product with the gridded observations across both the training data (Figure 2a) and independent withheld data (Figure 2b) demonstrates fits with an MAE less than 30 μatm and RMSE of around 40 μatm. The mean bias is negligible over the full range (< 0.2 μatm, smaller than observational uncertainty; Section 3.3). 70% of the calculated residuals fall within the -20 to 20 μatm range, while 47% of the grid cells have absolute residuals < 10 μatm especially further offshore (supplementary Figure S5). Despite seasonal and annual biases in observations (Figure 1; Section 2.1), our product performs similarly across different months and years (supplementary Table S1). The ANN ensemble model mean demonstrated improved performance compared to each individual ensemble member (supplementary Figure S6; supplementary Text S4).

Larger bias exists at the upper and lower limits of the gridded pCO_2 observational range. Our product underestimates pCO_2 observations greater than the 90th percentile (> 412 μatm; mean bias = -28 μatm), and overestimates values less than the 10th percentile (< 306 μatm; mean bias = 13 μatm). The spatial structure of the residuals reflects this bias distribution (supplementary Figure S5), with negative residuals in the strong mixing regions of the Salish Sea commonly characterized by high pCO_2 (Evans et al., 2012, 2019; Jarníková, Ianson, et al., 2022), and positive residuals along the upwelling zone off the west coast of Oregon and Washington States characterized by low pCO_2 (Evans et al., 2011). Observation-based pCO_2 products commonly overestimate pCO_2 in highly biologically productive coastal upwelling regions (Chau et al., 2022; Hales et al., 2012; Roobaert et al., 2024; Sharp et al., 2022). Chlorophyll (Table 1) as a proxy for biological productivity in training may not fully represent biological control on pCO_2. Ford et al. (2022) showed that in regions with high biological activity and nutrients supplied from depth (i.e., South Atlantic upwelling mesoscale eddies) regional, algorithm-derived net community production estimates (Ford et al., 2021) improved ANN pCO_2 estimates. Creation of coastal, regionally specific net community production algorithms, and inclusion as a predictor variable, may help reduce bias of low pCO_2 values in our study area.

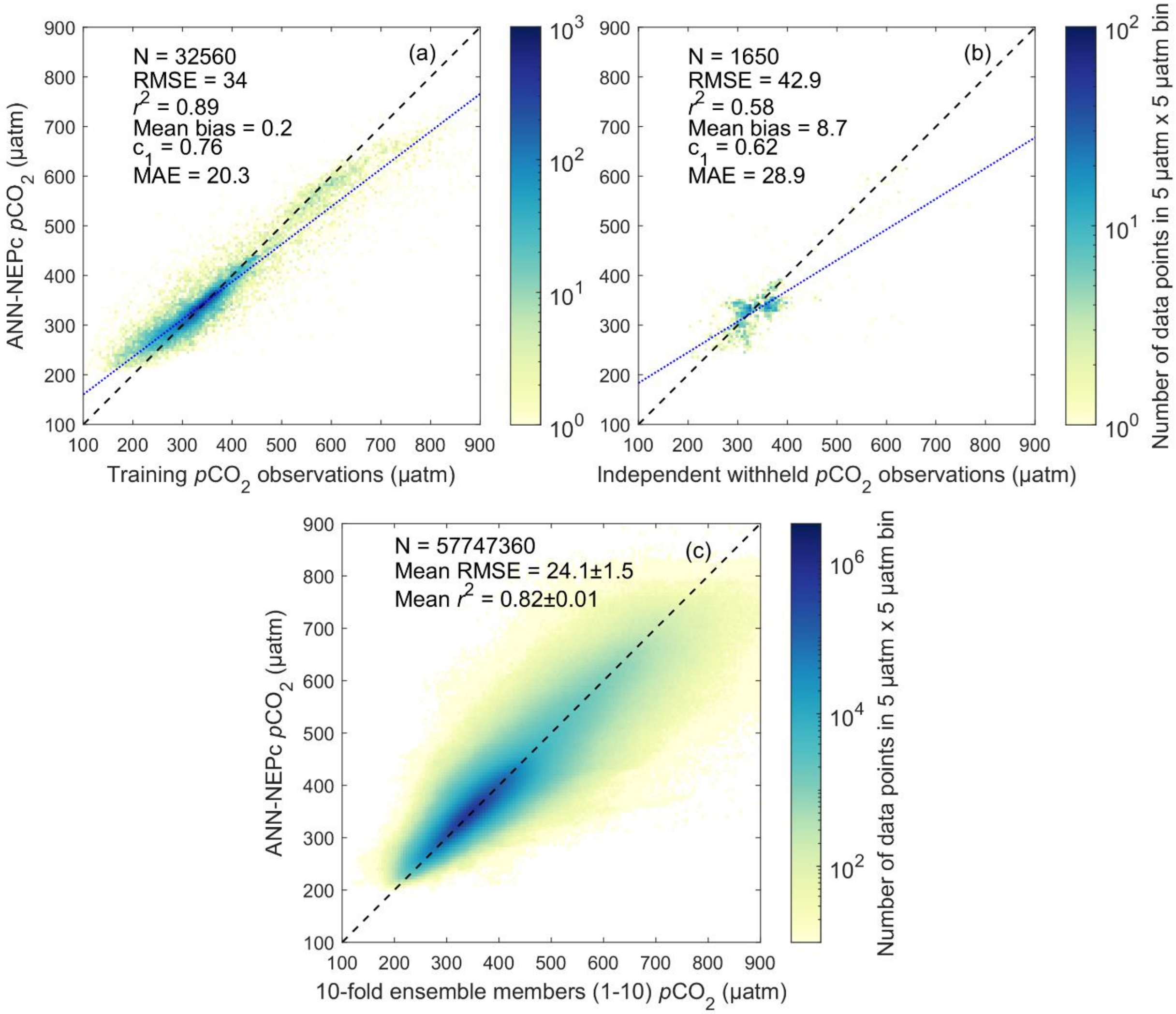

Figure 2. Our ensemble mean pCO_2 estimate (ANN-NEPc) against (a) observed pCO_2 training data, (b) observed pCO_2 independently withheld data, and (c) individual ensemble member estimates. Data are binned into 5 µatm by 5 µatm bins with data density shown in the colorbar on a log scale (note order of magnitude difference between panels). Dashed black line is the 1:1. Dotted blue line is the least squares best fit. Also shown are number of observations (N), root mean squared error (RMSE), coefficient of determination (r^2), mean absolute error (MAE), mean bias (calculated as the mean residual), and the slope of the linear regression (c_1).

In relative terms, our pCO_2 product performs nearly as well as an open ocean product, even nearshore (Table 2). Nearshore pCO_2 exhibits a much larger range of variability compared to the continental shelf and the offshore marine environment. Table 2 displays relative percent error (RPE) binned by distance offshore (d) calculated as:

$$\mathrm{RPE}_d = \mathrm{RMSE}_d / [\mathrm{prctile}_{95}(pCO_{2\,d}^{obs}) - \mathrm{prctile}_5(pCO_{2\,d}^{obs})] \times 100, \qquad (2)$$

where RMSE_d is the RMSE from gridded observational data averaged over the distance bin, $\mathrm{prctile}_{95}\left(p\mathrm{CO}_{2\,d}^{obs}\right)$ is the 95th percentile observed pCO_2 in that distance bin and $\mathrm{prctile}_{5}\left(p\mathrm{CO}_{2\,d}^{obs}\right)$ is the 5th percentile. Compared to a high-performance, regional open ocean product (Table 2; Duke, Hamme, et al., 2023a), RMSE increases moving toward shore but so does the range in pCO_2 such that the RPE is constant within a factor of two.

Table 2. Error statistics for our ensemble mean pCO_2 estimate against all gridded observation data binned by distance offshore: number of observations (N) per bin, observed range of variability (range; difference between the 95th and 5th percentile), root mean squared error (RMSE), and relative percent error (RPE; Eq. 2).

Distance offshore (km)	**N**	**Range (μatm)**	**RMSE (μatm)**	**RPE (%)**
0-25 (nearshore)	8669	481	54	11
25-50	4763	215	33	16
50-100	5770	153	24	15
100-150	3324	114	16	14
150-200	3317	90	12	13
200-300	6501	106	10	10
High-resolution Northeast Pacific open ocean product (Duke, Hamme, et al., 2023a)				
> 300	34096	83	7	8

3.2 Comparison to other products

Our pCO_2 estimate agrees well with one other Northeast Pacific coastal ocean estimate but diverges from coarser resolution global products (supplementary Figure S7). The regional Sharp et al. (2022) product within the northern extension of the California current system (45 °N to 59 °N, east of 140 °W) is nearly equivalent to our pCO_2 product within reported uncertainties (r^2 = 0.57; supplementary Figure S7a). However, our product produces estimates closer to shore (Section 5.2 below). Compared to our product and *in situ* observations, a global coastal climatology (Landschützer, Laruelle, et al., 2020; Laruelle et al., 2017) and multiyear product (Roobaert et al., 2024) do not capture the same pCO_2 range (supplementary Figure S7c&e; supplementary Figure S8). For example, both global products underestimate winter pCO_2 values closer to shore in the coastal Gulf of Alaska region (> 52 °N & < 50 km offshore; area-averaged climatological winter pCO_2 of 300 μatm and 290 μatm respectively compared to 330 μatm in this study; supplementary Figure S7d&f), highlighting the importance of finer resolution in coastal systems. This region also has the scarcest pCO_2 observations within our study area (0.37% coverage; Figure 1). Global SOM clusters commonly group the California current system with the Northwest European shelf and Sea of Japan (Laruelle et al., 2017; Roobaert et al., 2024). FFN non-linear relationships inside such clusters may not be suitable for regionally specific processes dominated by downwelling (Stabeno et al., 2004), glacial runoff (Pilcher et al., 2018; Siedlecki et al., 2017), significant seasonal biological productivity (Coyle et al., 2012; Fiechter & Moore, 2009; Hermann et al., 2009), and the influence of the upwelling subpolar Alaskan Gyre (Duke, Hamme, et al., 2023b; Hauri et al., 2021). This finding supports the Sharp et al. (2022) recommendation of increasing the number of SOM clusters for observation-based coastal ocean pCO_2 estimates to capture more regionally specific non-linear relationships, cognizant of SOCAT observation data density.

3.3 Uncertainty estimate

Uncertainty in the ANN-NEPc estimated pCO_2 product was determined following Duke, Hamme, et al. (2023b). The overall pCO_2 product uncertainty (θpCO_2 = 49 µatm in our coastal product) is calculated from the square root of the sum of the four squared errors: observational uncertainty based on reported SOCAT QA/QC flags (θ_{obs} = 3.7 µatm), gridding uncertainty based on the average standard deviation from gridding observations into monthly 1/12°x1/12° bins (θ_{grid} = 22.4 µatm; with an increasing gradient shoreward), ANN interpolation uncertainty based on the RMSE comparing the ANN-NEPc estimated pCO_2 to independent withheld data (θ_{map} = 42.9 µatm; Section 3.1), and ANN run randomness uncertainty based on the mean standard deviation between 10-fold ensemble members (θ_{run} = 6.8 µatm; supplementary Figure S9). ANN interpolation uncertainty is the largest contribution overall. Combining the reported uncertainty in the gas transfer velocity (Section 2.6) and the overall pCO_2 product uncertainty yields an average uncertainty of ±0.18 mol-C m^{-2} yr^{-1} in the air-sea gas flux across all grid cells, with the largest fraction of the error stemming from the uncertainty in the gas transfer velocity.

Our reported total uncertainty may appear high relative to other coastal pCO_2 products, but we include higher variability regions and more stringent error estimates. Other observation-based interpolated pCO_2 products in the coastal ocean report lower uncertainty values (RMSE values generally between 10 and 35 µatm in regional estimates detailed in S. Chen et al., (2016); 29 µatm globally in Roobaert et al. (2024); approximately 30 µatm in the California current system in Sharp et al. (2022); 55 µatm in the coastal subpolar Pacific in Chau et al. (2022)). However, most other estimates did not use independent withheld data to report total product uncertainty. Roobaert et al. (2024) point out their largest RMSE values are calculated along the Cascadia Shelf in our study area (62 µatm). Our pCO_2 product is also the only estimate that includes the nearshore, introducing higher variability (Table 2). Excluding the nearshore across all components of the uncertainty calculation yields an overall uncertainty of 40 µatm, more comparable to other coastal ocean estimates.

4.0 Comparison to high-resolution observations

Comparison to *in situ* observations shows that our ANN-NEPc estimated pCO_2 product resolves seasonal variability and broad spatial patterns well. Despite high spatial resolution, our design of a monthly timestep product means the ANN cannot reproduce short temporal (e.g., days) events. Predictor variable inaccuracy also contributes to pCO_2 estimate uncertainty, particularly in the nearshore where data assimilation into reanalysis models is limited (e.g., SSS and coastal limitations of Argo float array) and retrieval issues affect satellite estimates (e.g., SST and cloud masking, impact of aerosols, diurnal variability, uncertainty estimation, and validation). *In situ* measurements show that biogeochemical and hydrographic variability in our region occurs on spatial scales of less than 20 km (Nemcek et al., 2008), with spatial autocorrelation lengths increasing offshore (Murphy et al., 2001), and timescales of days to weeks (Evans et al., 2011, 2012, 2019; Fassbender et al., 2018). Our product is constrained by initial binning of observations to 1/12°x1/12° (approximately 9 km by 5 km) and a monthly time step, as well as scarcity of observations used to train (Figure 1). Comparing it directly with *in situ* mooring and shipboard underway pCO_2 system measurements in the coastal zone provides insight into when and where the ANN is both capable and incapable of resolving variability.

Our pCO_2 estimate captures the observed seasonal cycle (phase and amplitude) at regional mooring time series sites well (Figure 3; full time series at all five regional mooring sites in supplementary Figure S8). At NOAA's Gulf of Alaska Ocean Acidification (GAKOA) site south of Alaska's Kenai Peninsula, our product tends to overestimate seasonal summer minima and winter maxima values. However, it captures seasonal cycle timing well with a similar average seasonal amplitude even when not all mooring data are included in SOCATv2021 (this study = 144 µatm; GAKOA = 169 µatm; Figure 3b). At another NOAA Gulf of Alaska mooring site south of Kodiak Island, our estimate also captures the phase of the seasonal cycle well (r^2 = 0.89; N = 31 months; supplementary Figure S8a).

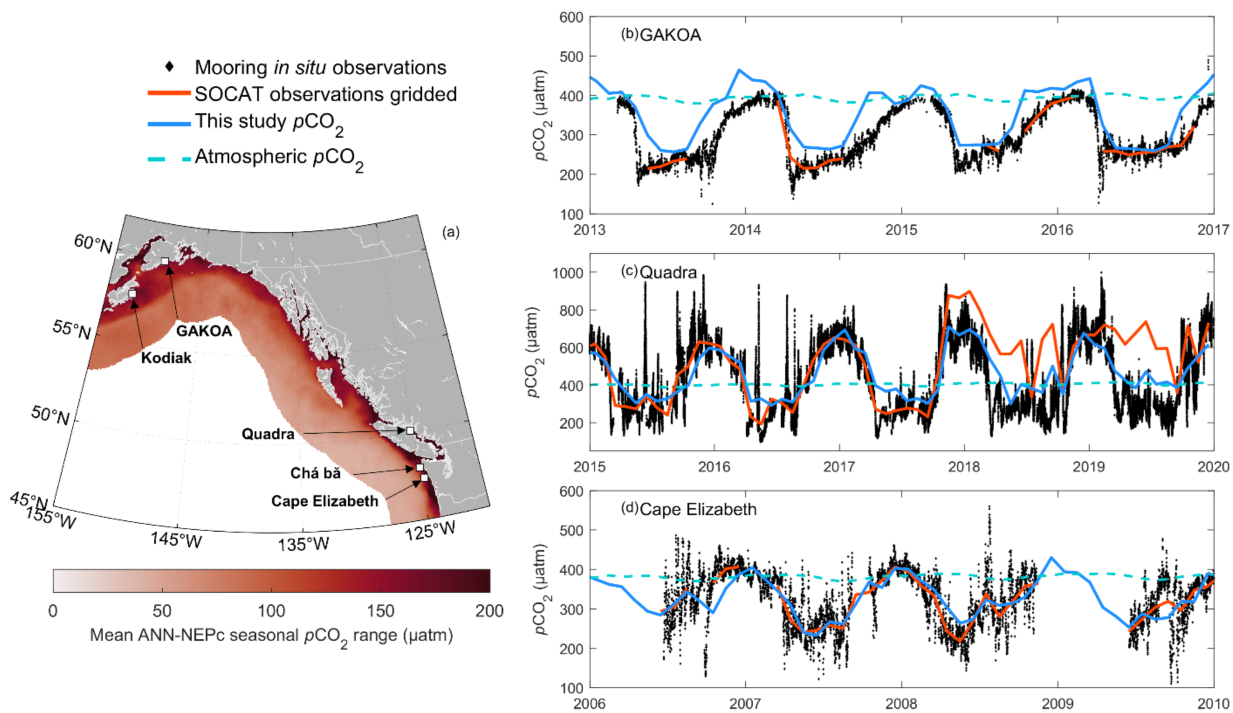

Figure 3. (a) Map of mean estimated surface ocean pCO_2 seasonal amplitude (1998-2019; range; annual maximum minus minimum) in µatm. Nearshore mooring time series at (b) Gulf of Alaska Ocean Acidification mooring (GAKOA), (c) Quadra, and (d) Cape Elizabeth mooring in situ pCO_2 data (black diamonds; not all included in SOCATv2021) plotted with co-located gridded SOCATv2021 (orange solid line), this study pCO_2 (blue solid line), and atmospheric pCO_2 (light blue dashed line). Kodiak and Chá bă and Roobaert et al. (2024) comparison time series in supplementary Figure S8.

The ANN recreates the seasonal cycle well at Hakai Institute's Quadra Island Station, but its monthly timestep does not capture higher frequency variability (Figure 3c). In some instances, measured pCO_2 at the Quadra mooring increases over 500 µatm within three days (e.g., June 9-12, 2015), leading to a strong outgassing signal. The ANN monthly estimate does not capture such short events. Monthly binning impacts net annual air-sea CO_2 fluxes within a single grid cell (2015 mean annual flux from daily mooring pCO_2 and wind speed: 0.08 mol m^{-2} yr^{-1}; compared to this study: 0.26 mol m^{-2} yr^{-1}) but likely has a smaller impact when quantifying the larger regional flux. Near the end of the time series (late 2017 to 2020), the gridded SOCAT data deviates from the *in situ* mooring data due to inclusion of nearby shipboard data, yet our estimated pCO_2 continues to better represent the mooring seasonal cycle. When evaluating ANN performance (Section 3.1), this difference from the gridded observation data contributes to a higher measure of uncertainty, yet in situ representation is still preserved compared to the mooring data.

The ANN does capture part of the signal from somewhat longer (i.e., weeks) summer high pCO_2 events at NOAA's Cape Elizabeth mooring off the west coast of Washington State (Figure 3d). Horizontal advection of freshwater (July 2007) or upwelling events (> 500 μatm; July 2008; Evans et al., 2015) can cause high summer pCO_2 values. These extreme events impact bin-averaged training data, allowing the ANN to recover some of the short duration signal, albeit at a lower value. Our product reproduces both persistent, weeks long events < 35 km offshore, in line with the monthly averaged observations.

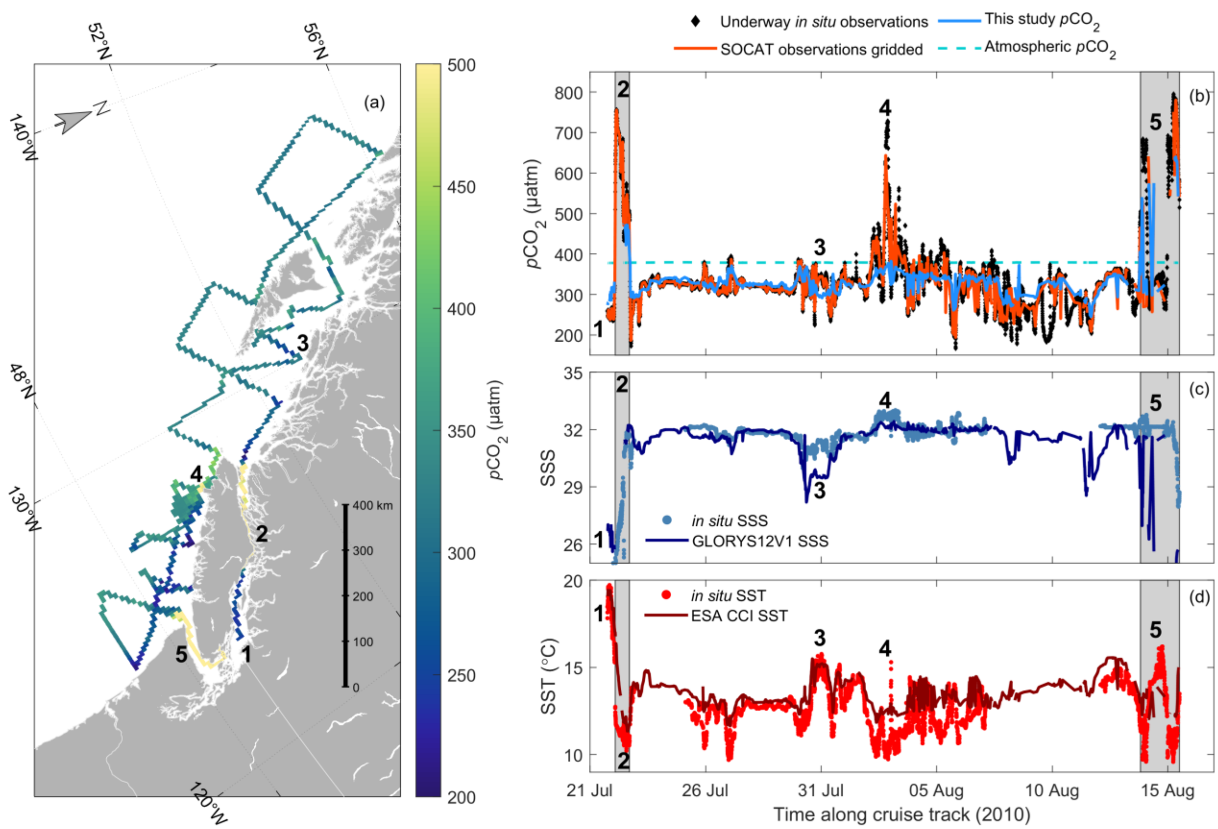

Figure 4. (a) pCO$_2$ along 2010 West Coast Ocean Acidification cruise track from 21 Jul 2010 to 15 Aug 2010 (Evans et al., 2012). Data is gridded into 1/12° by 1/12° bins. Events indicate (1) cruise start, (2) Johnstone Strait, (3) Hecate Strait, (4) intense upwelling plume near Brooks Peninsula, and (5) Juan de Fuca Strait respectively. Subplots against time along cruise track for (b) pCO$_2$ where underway in situ pCO$_2$ data (black diamonds) are plotted with co-located monthly gridded data (orange solid line), this study pCO$_2$ (blue solid line), and atmospheric pCO$_2$ (light blue dashed line). (c) Sea surface salinity (SSS) with underway in situ SSS (light blue dots) and co-located reanalysis SSS (dark blue solid line; used as a predictor variable). SSS values near cruise start as low as 15 in situ and 24 from reanalysis (not shown). (d) Sea surface temperature (SST) with underway in situ SST (red dots) and co-located satellite-based SST (dark red solid line; used as a predictor variable). Gray boxes highlight tidal mixing zones (e.g., Johnstone Strait, Juan de Fuca and Haro Straits and connecting waters).

Direct comparison to a cruise from July/August 2010 provides another example of our pCO$_2$ product's ability to capture broadscale patterns. The ANN estimate resolves undersaturated pCO$_2$ conditions in the Salish Sea at the start of the cruise well (point 1; Figure 4). Through Johnstone Strait (50.5 °N, 126.5 °W), a strong tidal mixing zone (Evans et al., 2022), lack of predictor data coverage prevents estimation of pCO$_2$ in those grid cells at all (point 2; Figure 4). The ANN captures the lower variability continental shelf and slope environment in Queen Charlotte Sound and around Haida Gwaii well (between points 2 and 4; Figure 4). Differences between estimated and observed pCO_2 exist in Hecate Strait (point 3; Figure 4) likely due to strong underestimation of SSS as a predictor in the reanalysis product (point 3; Figure 4c). Along the west coast of Vancouver Island, shipboard observations captured an upwelling event off Brooks Peninsula (50.14 °N, 127.78 °W; Asher et al., 2017), visible in decreased temperatures, elevated salinity, and very high *in situ* pCO_2 (point 4; Figure 4). The ANN does not replicate this short upwelling event (i.e., days; Asher et al., 2017). High pCO_2 driven by tidal mixing in the Juan de Fuca and Haro Straits are captured by the ANN (point 5; Figure 4; Jarníková, Olson, et al., 2022). An abundance of consistently high pCO_2 observations results in a strong reconstruction by the ANN in this region (Evans et al., 2012).

5 Air-sea CO_2 flux and pCO_2 drivers

Long-term (1998–2019) mean air-sea CO_2 fluxes display a pronounced juxtaposition between strong uptake and outgassing regions in the coastal Northeast Pacific Ocean (Figure 5c). Overall, air-sea CO_2 flux estimates from our product show this coastal zone acts as a net sink for atmospheric CO_2, drawing down 0.96±0.25 Tg C yr^{-1} with a mean flux of -0.7 mol m^{-2} yr^{-1} but high variability with a standard deviation of 1.4 mol m^{-2} yr^{-1}. Mean pCO_2 and air-sea CO_2 fluxes display similar patterns, with high pCO_2 nearshore leading to outgassing and low pCO_2 along the transition zone and continental shelf environments taking up atmospheric CO_2 (Figure 5a&c). Canada's West Coast exclusive economic zone has a CO_2 uptake of 0.61±0.11 Tg C yr^{-1}. Compared to the open ocean region of the Northeast Pacific (Duke, Hamme, et al., 2023b), the adjacent coastal ocean is a weaker sink for atmospheric CO_2 by area (40% weaker compared to -1.2 mol m^{-2} yr^{-1} in the open ocean), taking up 64% less CO_2 total within 40% less area (open ocean uptake = 2.63±0.53 Tg C yr^{-1}; open ocean surface area = $1.8x10^6$ km^2; coastal ocean surface area = $1.1x10^6$ km^2). Elevated pCO_2 and outgassing is also reported in the subpolar Alaskan Gyre system (Figure 5a&c), consistent with Duke, Hamme, et al. (2023b).

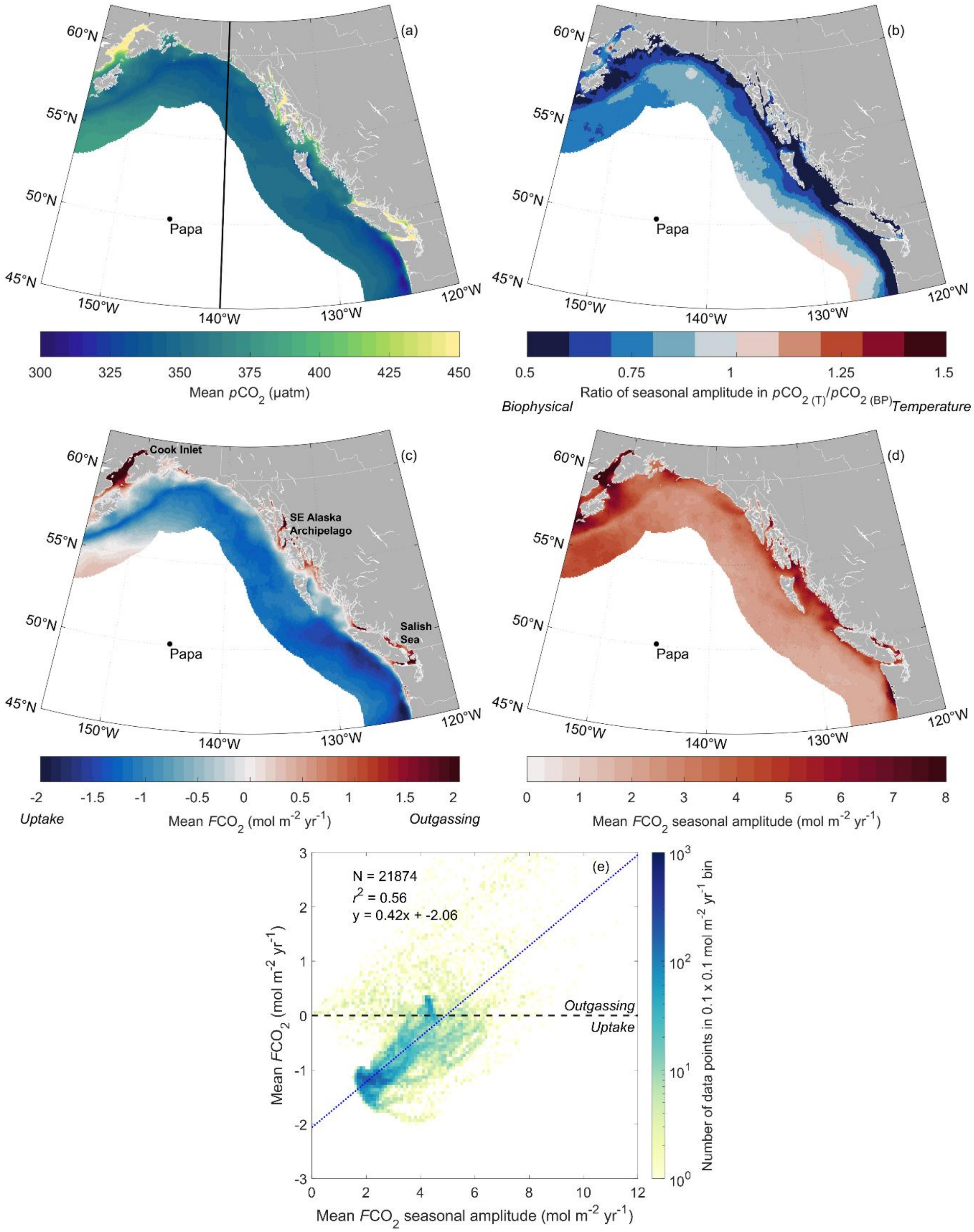

Figure 5. (a) Mean pCO_2 (1998-2019) in μatm. 140 °W meridian divide used in Section 5.2 analysis shown for reference. (b) Ratio of pCO_2 seasonal amplitude in thermal component (i.e., changes due to temperature; $pCO_{2\,(T)}$) and biophysical component (i.e., changes due to circulation, mixing, gas exchange, and biology; $pCO_{2\,(BP)}$). (c) Mean air–sea CO_2 flux (1998-2019) in mol m^{-2} yr^{-1}. Negative flux values indicate CO_2 uptake by the ocean. (d) Mean air-sea

CO_2 flux seasonal amplitude (range; annual maximum minus minimum) in mol m^{-2} yr^{-1}. (e) Mean air-sea CO_2 flux vs. mean air-sea CO_2 flux seasonal amplitude (grid cell by grid cell). Dotted blue line is the least squares best fit. Dashed black line separates values of outgassing (positive) from uptake (negative).

5.1 Regional patterns

Spatially, the study area can be divided into four distinct regions based on air-sea CO_2 flux patterns in our product. The net annual air-sea CO_2 flux is anti-correlated with the mean air-sea CO_2 flux seasonal amplitude (r^2 = 0.56; p < 0.01; Figure 5e). We identify four regions that drive this pattern from most offshore to inshore: the transitional zone connecting the open ocean and the coast is a net sink with a small seasonal cycle, the Cascadia Shelf where the net sink is even stronger but the seasonal cycle remains low, nearshore regions with large seasonal cycles, and semi-enclosed estuaries with strong outgassing. To further disentangle driving processes between these four regions we decompose the estimated pCO_2 into a thermal ($pCO_{2\ (T)}$) and biophysical ($pCO_{2\ (BP)}$) component (supplementary Text S5; Takahashi et al., 1993, 2002). We then take the ratio ($R_{T\ BP}^{-1}$) of the seasonal amplitude (climatological maximum minus minimum) of the two components ($pCO_{2\ (T)}/pCO_{2\ (BP)}$; Figure 5b), where biophysical processes dominate if $R_{T\ BP}^{-1}$ is less than one and vice versa.

Much of the offshore transitional zone (medium blue colours in Figure 5c) acts as a sink for atmospheric CO_2 year-round where thermal and biophysical pCO_2 components are nearly balanced. Low air-sea CO_2 flux seasonal amplitudes in the transitional zone (> 50 km offshore; excluding the subpolar Alaska Gyre) correspond to net annual atmospheric CO_2 uptake. In the southeast of the study area (Figure 5b), the North Pacific Current region experiences a relative balance of opposing thermal and biophysical pCO_2 components seasonally ($R_{T\ NT}^{-1}$ approximately = 1; Duke, Hamme, et al., 2023b; A. J. Sutton et al., 2017; Takahashi et al., 2006; Wong et al., 2010). Along most of the transitional zone where $R_{T\ NT}^{-1}$ is closer to one (Figure 5b), we also report low pCO_2 seasonal amplitudes (Figure 3a) allowing for continuous pCO_2 undersaturation with respect to the atmosphere and continuous annual uptake with low air-sea CO_2 flux seasonal amplitudes (supplementary Figure S12; Figure 5d). Advection of low pCO_2 (Duke, Hamme, et al., 2023b; Takahashi et al., 2006) water by the North Pacific Current from the open ocean toward the coast causes overall pCO_2 undersaturation in this region (Reed & Schumacher, 1986; Thomson, 1981; Weingartner et al., 2002). The low pCO_2 amplitudes are maintained by the effect of temperature on pCO_2 (increasing during warming and decreasing during cooling) dampening changes due to spring phytoplankton blooms (drawing down pCO_2) and winter surface mixed layer deepening (increasing pCO_2).

The most prominent CO_2 sink region is found along the Cascadia Shelf, inshore of the transitional zone, with a mean flux of -1.5 mol m^{-2} yr^{-1} (darkest blue colours in Figure 5c). Along the continental shelf and within much of the nearshore, biophysical processes (e.g., coastal upwelling, seasonal biological drawdown, mixing) dominate the seasonal cycle of pCO_2 with R_T $_{NT}^{-1}$ values < 1. Summer upwelling fuels primary productivity causing surface pCO_2 drawdown as waters are advected offshore (Hales et al., 2005; Teeter et al., 2018; Ware & Thomson, 2005). Winter downwelling drives onshore transport of low pCO_2 offshore waters and prevents subsurface waters, with elevated respiratory CO_2, from mixing to the surface (i.e., coastal nutrient trap; Ianson et al., 2009; F. A. Whitney et al., 2005; Wilkerson & Dugdale, 1987). This general circulation of shelf waters maintains low seasonal flux amplitudes and strong CO_2 uptake on the Cascadia Shelf.

Much of the nearshore tends to experience seasonally strong, juxtaposing air-sea CO_2 fluxes, leading to near zero net annual CO_2 fluxes (nearshore white colours in Figure 5c). For example, closer to shore north of 50 °N and south of the Southeast Alaska Archipelago, winter mixed layer deepening brings water rich in nutrients and CO_2 from respired organic matter to the surface, increasing pCO_2, leading to strong CO_2 outgassing to the atmosphere when light is limiting (supplementary Figure S12a; Marchese et al., 2022). In the spring, substantial primary productivity draws down pCO_2 (Marchese et al., 2022), reverting the region to a prominent sink for atmospheric CO_2 (supplementary Figure S12b). This large seasonal amplitude results in a net neutral flux.

Semi-enclosed, nearshore estuarine environments display strong CO_2 outgassing in our product, that is not always observed in regional high-resolution models. High pCO_2 values and outgassing fluxes (mean CO_2 flux of 0.7 mol m^{-2} yr^{-1}) occur in Cook Inlet, the Salish Sea, and the Southeastern Alaska Archipelago (Figure 5c). Globally, the source strength of these integrated estuarine environments is comparable to (or smaller than) other nearshore source regions that decrease averaged coastal ocean CO_2 uptake (Section 5.2 below; Duke, Richaud, et al., 2023; Fennel et al., 2019; Laruelle et al., 2018). In high-resolution regional models, the Salish Sea has been reported as a weak net annual source (this study: 1.0 mol m^{-2} yr^{-1};

comparable to Jarníková, Ianson, et al. (2022): 0.69 mol m^{-2} yr^{-1}), and Cook Inlet as a net sink (Hauri et al., 2020; Pilcher et al., 2018). Limited observations used to constrain both our observation-based estimate and regional models may create discrepancies between them. Our estimate is based on all available surface ocean pCO_2 observations along with a suite of predictor variables (Figure 1; Table 1), whereas regional process-based models using data for boundary conditions simplify and parameterise mechanisms (Hauri et al., 2020; Jarníková, Ianson, et al., 2022; Pilcher et al., 2018). Global observation-based estimates and models also disagree, where model fluxes are often more negative (stronger sink) at northern latitudes, attributed to a smaller seasonal pCO_2 amplitude (Resplandy et al., 2024).

5.2 Nearshore fluxes

The nearshore coastal environment (0 - 25 km offshore) exhibits large air-sea CO_2 fluxes, over a relatively small surface area, impacting regional marine carbon budgeting. As our estimate wraps around the coast from primarily E-W to primarily N-S, we split the region along the 140 °W meridian (Figure 5a). Averaging grid cells approximately parallel to the regional coastline along longitudinal bands (155 °W to 140 °W west of 140 °W; Figure 6a&b) and along latitudinal bands (56 °N to 45 °N east of 140 °W; Figure 6c&d), the inclusion or exclusion of the nearshore environment creates large differences in estimated net annual air-sea CO_2 fluxes, for example, between 154 °W to 149 °W encompassing Cook Inlet (absolute flux difference of 250%, switching from a net sink to a source; Figure 6b). North to south from 56 °N to the northern extension of the California current system at 45°N (Figure 6d), including the nearshore leads to a slightly weaker net annual sink for atmospheric CO_2. The difference is largest within latitudinal bands inclusive of the Salish Sea (49-51 °N; 20% weaker). Differences in zonally averaged pCO_2 and air-sea CO_2 fluxes also exist between products with varying nearshore coverage (Section 3.2; Roobaert et al., 2024; Sharp et al., 2022). Basin-wide, inclusion of the nearshore changes the annual exchange with the atmosphere within the study area by 0.06 Tg C yr^{-1} (6%). These results highlight the importance of including the nearshore in regional marine carbon budgets.

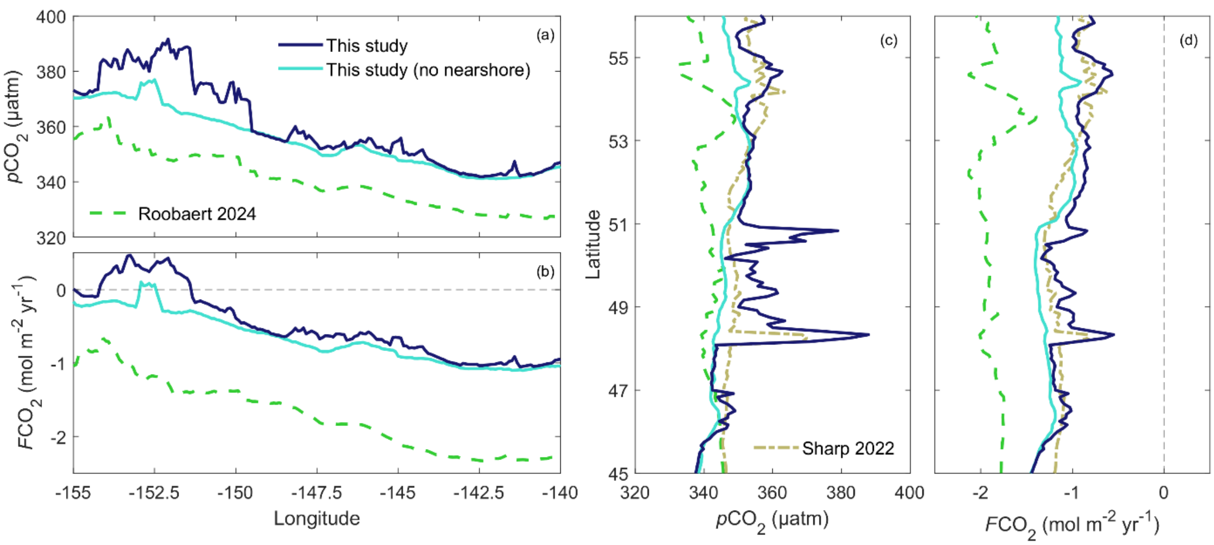

Figure 6. Longitudinally averaged estimates west of 140 °W of mean (a) pCO_2 and (b) air-sea CO_2 flux of: this study (dark blue), this study removing the nearshore (cyan). (c) and (d) are latitudinally averaged estimates east of 140 °W respectively. Additional observation-based estimates with overlapping domains including: Sharp et al. (2022) (dot-dash beige), and Roobaert et al. (2024) (dashed lime green). Sharp et al. (2022) air-sea CO_2 fluxes calculated following Section 2.6.

5.3 Dominant controls on variability

Four distinct tiers of predictor variable importance rankings emerged from a perturbation-based spatial sensitivity analysis in estimated pCO_2 (Figure 7a). The ANN is purely a set of empirical, not mechanistic, relationships between pCO_2 observations and predictor variables, though variables were selected with mechanism in mind (Table 1). We used a perturbation-based spatial sensitivity analysis (Section 2.5) to probe the dependency of the ANN relationships on each variable, as they cannot be viewed directly (unlike a multiple linear regression). Atmospheric pCO_2 and atmospheric pCO_2 anomaly (removing the seasonal cycle; Section 2.2) are the most important predictors, followed by SST, and then process-driven controls whose importance varies spatially. Atmospheric pCO_2 and atmospheric pCO_2 anomaly are the only two predictor variables that capture a trend in time from 1998 to 2019 (i.e., increase of 2.12 μatm yr^{-1} due to anthropogenic emissions). Due to the trend, these variables also experienced the largest absolute value perturbation (mean basin-wide increase of 7 μatm), at least one order of magnitude greater than other variables. The third most important predictor for estimating pCO_2 is SST. Basin-wide, the sensitivity test introduced a mean SST increase of 1.5 °C, resulting in a mixed pCO_2 response where generally there was a decrease, outside of the Gulf of Alaska central glacial drainage basin where pCO_2 increased (supplementary Figure S13a). This result does not follow the mechanistic reduced solubility of CO_2 in warmer water. However, it emphasizes the importance of the SST seasonal cycle as a predictor (strong correlation, typically negative, between pCO_2 and SST; supplementary Figure S13b).

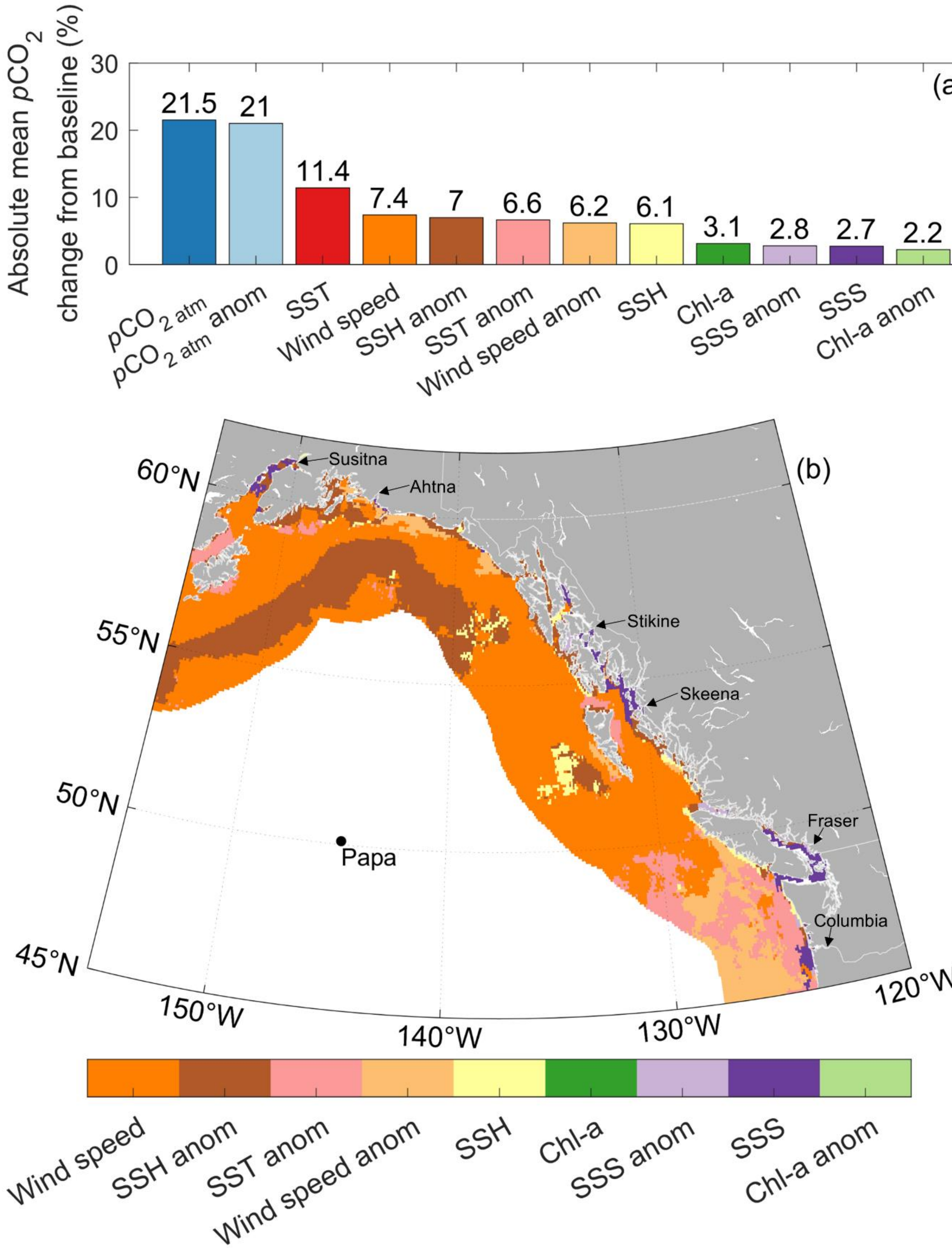

Figure 7. (a) Predictor variables ordered by absolute mean pCO_2 change from baseline run during perturbation-based spatial sensitivity analysis (Section 2.5). (b) Most dominant process-based predictor variable mapped by largest absolute mean pCO_2 change from baseline run during perturbation-based spatial sensitivity analysis (excluding top three variables from (a)). No grid

cells displayed Chl or Chl anomaly as the largest absolute mean pCO_2 change from baseline over the full study time range (1998-2019). Major river outflows are labelled for reference.

Excluding the three most dominate controls (atmospheric pCO_2, atmospheric pCO_2 anomaly, and SST), the spatial distribution of predictor variable importance rankings can be explained by mechanistic drivers even though the ANN is purely empirical. SSH anomaly is important along the Alaskan Gyre boundary, where the upwelling gyre exerts control over local biogeochemistry (Figure 7b; Duke, Hamme, et al., 2023b; Hauri et al., 2021). Wind speed (as a proxy for mixed layer depth) is important throughout most regions along the continental shelf and the outer coast as winter mixed layer deepening brings CO_2-rich subsurface waters to the surface (mean basin-wide increase of 0.4 m s^{-1} resulting in a pCO_2 increase of 1.7%; Figure 7b). SSH and SSH anomaly are additionally important offshore of Sitka, Alaska (57 °N, 143 °W) and Haida Gwaii (52 °N, 133 °W) where mesoscale anticyclonic eddies with enhanced primary productivity and high SSH propagate away from the continental margin (Figure 7b; Batten & Crawford, 2005; Crawford et al., 2007; Crawford & Whitney, 1999; F. A. Whitney et al., 2005; F. Whitney & Robert, 2002). In the North Pacific Current influenced region southeast of the study area, SST anomaly and wind speed anomaly are the most important predictors linked to the relative balance of opposing mechanisms (i.e., thermal and biophysical pCO_2 components; Figure 5b).

Nearshore regions experience a range of predictors with prominent features mostly controlled by salinity (SSS and SSS anomaly) in coastal estuarine areas (Figure 7b), and tidally mixed areas (e.g., Juan de Fuca Strait, Johnstone Strait; Figure 4a). In additional regions where freshwater discharge is important (e.g., supplementary Table S2), SSH and SSH anomaly emerge as important predictors potentially linked to discharge associated changes to nearshore sea level (Figure 7b; Durand et al., 2019). Neither perturbation to Chl nor Chl anomaly resulted in the largest absolute mean pCO_2 change from baseline over 264 months in a single grid cell (Figure 7b). However, seasonally Chl emerges as a prominent predictor in scattered grid cells along nearshore West Coast Vancouver Island and in the Southeast Alaska Archipelago during the spring (i.e., March, April, and May; not shown).

5.4 Air-sea pCO_2 trends

Trends in the last decades (1998-2019) in ΔpCO_2 (sea – air) display spatial heterogeneity in the coastal Northeast Pacific, with a gradient of smaller trends moving offshore. A linear fit was applied to the ΔpCO_2 anomaly time series within each grid cell to calculate the trend and standard error (i.e., deseasonalized; Section 2.2). Regions that experience an increase in surface ocean pCO_2 close to the increase in atmospheric (i.e., resulting in a small ΔpCO_2 trend) are spatially distinct from those that have an insignificant trend in pCO_2 leading to a large divergence with the atmosphere (i.e., large ΔpCO_2 trend). Grid cells with a small ΔpCO_2 trend are dominantly located in the outer coast (> 50 km offshore) and in the southeast of the study area (Figure 8a). Trends are closer to the atmospheric trend in this region (2.12 μatm yr^{-1}), meaning any change in the carbon sink due to anthropogenic climate change will require long observation time series to detect, as the signal is small relative to internal variability (Gooya et al., 2023; McKinley et al., 2016; Resplandy et al., 2015; Adrienne J. Sutton et al., 2019). We report trends in pCO_2 that are similar to those observed at time series sites along Fisheries and Ocean Canada Line P stations (this study: P4 = 1.3±0.1 μatm yr^{-1}; P12 = 1.6±0.1 μatm yr^{-1}; comparable to Franco et al. (2021): P4 = 1.0±1.4 μatm yr^{-1}; P12 = 1.5±0.6 μatm yr^{-1}).

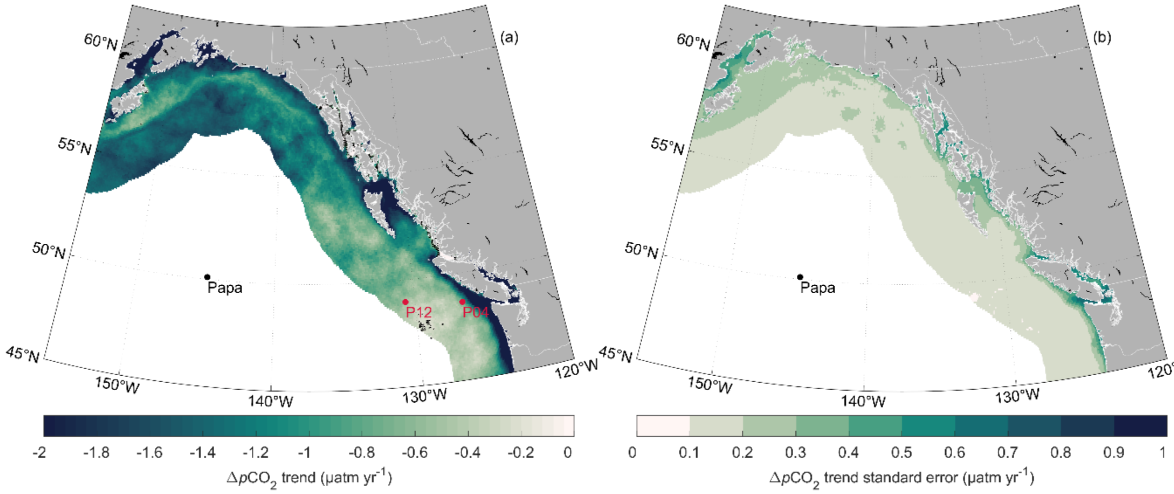

Figure 8. 1998-2019 trend in (a) $\Delta p CO_2$ anomaly (i.e., deseasonalized) where more negative (darker) values indicate an increase in air-sea pCO_2 disequilibria with time. Black crosshatches show grid cells with an insignificant calculated trend (outside the 95% confidence level; $p \geq 0.05$; 0.4% of total grid cells). (b) Standard error of the estimated slope in the $\Delta p CO_2$ trend fit.

Large $\Delta p CO_2$ trends (and low or insignificant pCO_2 trends) occur in regions experiencing strong connectivity to the older subsurface waters of the Northeast Pacific (e.g., subpolar Alaskan Gyre, west coast upwelling zone; Figure 8a). This older water has a lower anthropogenic carbon load (Carter et al., 2019; Clement & Gruber, 2018; Gruber et al., 2019; Sabine et al., 2004), which may be responsible for the lag in the increase in surface ocean pCO_2 (e.g., Duke, Hamme, et al., 2023b). The $\Delta p CO_2$ trend in the Alaska Gyre is dominated by the winter trend, whereas the west coast upwelling zone is dominated by the summer trend (supplementary Figure S14). These seasonal trends coincide with the timing of greatest connectivity to depth in each region. Strongest Alaskan gyre upwelling occurs in winter (Gargett, 1991; Talley, 1985), whereas the coastal upwelling season is spring and summer (Dorman & Winant, 1995; Hsieh et al., 1995) with downwelling occurring in the winter (Section 5.1; Thomson & Ware, 1996). In the nearshore (e.g., Southeast Alaska Archipelago, Salish Sea), subsurface waters exchange through estuarine flow and tidal mixing. In these regions, we report low or insignificant winter $\Delta p CO_2$ trends and large negative summer trends in agreement with regional model results (e.g., Jarníková, Ianson, et al., 2022). Increasing summer air-sea pCO_2 disequilibria enhances ocean CO_2 uptake, whereas winter air-sea disequilibria has remained relatively constant, maintaining ocean outgassing. In winter, light limits biological productivity, resulting in higher total CO_2 in the surface (Evans et al., 2019; Ianson et al., 2016; Simpson et al., 2022). This increase in total CO_2 reduces the buffer capacity of the carbonate system (Revelle & Suess, 1957), so that the pCO_2 increase due to anthropogenic carbon uptake is larger than it is in summer in many temperate zones (e.g., Jarníková, Ianson, et al., 2022; Landschützer et al., 2018). Our findings are consistent with global ΔpCO_2 trend estimates where most coastal regions appear to exhibit negative ΔpCO_2 trends (i.e., likely becoming stronger atmospheric CO_2 sinks or weaker sources; Fennel et al., 2019; Laruelle et al., 2018; Resplandy et al., 2024; Roobaert et al., 2024; Wang et al., 2017).

6 Conclusions

Our high-resolution, neural network created pCO_2 product reproduces observed coastal Northeast Pacific Ocean variability well, from the outer transitional zone to the nearshore (0 – 25 km offshore). We interpolated sparse observations using non-linear relationships developed with a neural network based on predictor data from satellite and reanalysis products to create a continuous, gridded monthly pCO_2 estimate at a 1/12° spatial resolution, inclusive of the nearshore. This pCO_2 product provides a baseline environmental context for pCO_2 and air-sea CO_2 flux variability in the study area with an uncertainty of 49 µatm and 0.24 mol-C m^{-2} yr^{-1}, respectively. The product resolves seasonal variability (phase and amplitude) and broad spatial patterns well compared to high-resolution *in situ* observations. The product is not designed to capture daily – weekly variability.

A unique ANN sensitivity analysis shows that variations in pCO_2 results agree with mechanistic drivers even though the ANN itself is purely empirical. ANNs are not based on predefined equations but their ability to capture information inherent to the training data, preventing any explicit explanation of how predictor variables and their output are related. We suggest a new systematic sensitivity analysis introducing perturbations to predictor variables, with a consideration for natural spatial variability, to produce mapped variable importance rankings. This approach offers insight providing greater transparency to ANN “black box” techniques.

We describe the coastal Northeast Pacific as a net sink for atmospheric CO_2 with large spatial heterogeneity between outgassing in the nearshore and uptake on the outer coast. Net annual air-sea CO_2 flux is largely anticorrelated with seasonal air-sea CO_2 flux amplitude. Patterns inherent to specific regions drive this anticorrelation, including circulation and opposing seasonal upwelling or relaxation vs. downwelling, and may make the relationship regionally specific rather than applicable to the wider global coastal ocean. Our results also emphasize the importance of including nearshore fluxes (often omitted by other coastal products), which are likely to be a source reducing the net coastal sink, when constructing marine carbon budgets (e.g., Legge et al., 2020). These findings could be potentially important considerations for reporting marine carbon dioxide removal approaches in the study area, as interventions impacting source areas are treated differently from those enhancing natural sinks (Verra, 2023).

Trends over the last decades show outer coast pCO_2 may be experiencing the largest increase in air-sea pCO_2 disequilibrium, due to strong connectivity with subsurface waters low in anthropogenic CO_2, while pCO_2 in the North Pacific Current region tracks increasing atmospheric pCO_2 more closely. Trends reported here across the coastal Northeast Pacific indicate most regions are likely to become stronger atmospheric CO_2 sinks or weaker sources.

Improving regional observational coverage and continuity and advancing the ANN approach will improve future air-sea CO_2 flux estimates. Some regions in the coastal Gulf of Alaska display large net annual air-sea CO_2 fluxes (e.g., Cook Inlet) yet are extremely sparsely monitored. A higher temporal resolution, such as daily, could enable the ANN to capture highly episodic air-sea CO_2 flux events common to the nearshore. However, this approach would dramatically reduce the percent coverage of observation training targets. A solution may be creating ANN non-linear relationships to interpolate pCO_2 directly from *in situ* observations. Using high frequency, collocated sensors and non-uniform “highest available resolution” satellite and reanalysis datasets for predictor variables not collected *in situ*, a higher temporal and/or spatial resolution coastal product could be developed without substantial loss in ANN training targets.

Acknowledgments

Funding for this project was provided by the Natural Sciences and Engineering Research Council of Canada (NSERC) through the Advancing Climate Change Science in Canada program (grant# ACCPJ 536173-18) to RH. Funding from Fisheries and Oceans Canada's Aquatic Climate Change Adaptation Service Program to DI supported the analysis of recent underway pCO_2 measurements made by the Line-P program (grant# 96036). PD financial support also provided by a Natural Sciences and Engineering Research Council of Canada (NSERC) Doctoral

Postgraduate Scholarship and the joint Fisheries and Oceans Canada (DFO) and National Oceanic and Atmospheric Administration (NOAA) Ocean Acidification Collaborative Funding Initiative.

The authors declare no conflicts of interest relevant to this study.

Fisheries and Oceans Canada (DFO) runs the Line P monitoring program. National Oceanic and Atmospheric Administration (NOAA) operates the Kodiak, Gulf of Alaska Ocean Acidification, Chá bă, and Cape Elizabeth moorings. Hakai Institute operates Quadra Island Station. We extend our thanks to Jamie Shutler and Dan Ford for their valuable brainstorming efforts regarding the $p\mathrm{CO_2}$ temperature correction section. We are grateful to Wiley Evans for sharing previously published $p\mathrm{CO_2}$ data from the 2010 West Coast Ocean Acidification cruise. We also want to thank Philippe Tortell and Robert Izett for providing previously published $p\mathrm{CO_2}$ data from the May 2007 and May 2010 La Perouse cruises.

Open Research

All data used is publicly available. ANN-NEPc $p\mathrm{CO_2}$ and air-sea CO_2 flux fields created for this publication are available through the National Center for Environmental Information (NCEI Record ID: BHE12VV0E). $p\mathrm{CO_2}$ data are from the Surface Ocean CO_2 Atlas (SOCAT) v2021 (available at https://www.socat.info/) as well as additional data from the Fisheries and Oceans Canada February 2019 Line P cruise, a West Coast Ocean Acidification cruise from July and August 2010 (Evans et al., 2012), and La Perouse cruises from May 2007 and May 2010 (available at https://www.waterproperties.ca/linep/). Sea surface temperature and chlorophyll-a are from the European Space Agency Climate Change Initiative (available at https://climate.esa.int/en/odp/#/dashboard). Sea surface salinity and sea surface height are from Copernicus Marine Environment Monitoring Service (available at https://data.marine.copernicus.eu/product/GLOBAL_MULTIYEAR_PHY_001_030/description). Ocean surface wind data at 10 m height are from Regional Deterministic Reforecast System (available at https://caspar-data.ca/; detailed here https://github.com/julemai/CaSPAr). Mooring data used in analysis are also available through the National Center for Environmental Information (NOAA moorings: NCEI Accession 0173932; and Hakai Institute Quadra Island Field Station: NCEI Accession 0208638).

References

Asher, E., Dacey, J. W., Ianson, D., Peña, A., & Tortell, P. D. (2017). Concentrations and cycling of DMS, DMSP, and DMSO in coastal and offshore waters of the Subarctic Pacific during summer, 2010-2011. *Journal of Geophysical Research: Oceans*, *122*(4), 2647–2651. https://doi.org/10.1002/2016JC012465.Received

Bakker, D. C. E., Pfeil, B., Landa, C. S., Metzl, N., O'Brien, K. M., Olsen, A., et al. (2016). A multi-decade record of high-quality fCO2 data in version 3 of the Surface Ocean CO2 Atlas (SOCAT). *Earth System Science Data*, *8*(2), 383–413. https://doi.org/10.5194/essd-8-383-2016

Batten, S. D., & Crawford, W. R. (2005). The influence of coastal origin eddies on oceanic plankton distributions in the eastern Gulf of Alaska. *Deep-Sea Research Part II: Topical Studies in Oceanography*, *52*(7–8), 991–1009. https://doi.org/10.1016/j.dsr2.2005.02.009

Bauer, J. E., Cai, W.-J., Raymond, P. A., Bianchi, T. S., Hopkinson, C. S., & Regnier, P. A. G. (2013). The changing carbon cycle of the coastal ocean. *Nature*, *504*(7478), 61–70. https://doi.org/10.1038/nature12857

Bélair, S., Roch, M., Leduc, A.-M., Vaillancourt, P. A., Laroche, S., & Mailhot, J. (2009). Medium-Range Quantitative Precipitation Forecasts from Canada's New 33-km Deterministic Global Operational System. *Weather and Forecasting*, *24*(3), 690–708. https://doi.org/10.1175/2008WAF2222175.1

Benway, H., Alin, S., Boyer, E., Cai, W. J., Coble, P., Cross, J., et al. (2016). A Science Plan for Carbon Cycle Research in North American Coastal Waters. Report of the Coastal CARbon Synthesis (CCARS) community workshop, August 19-21, 2014. Ocean Carbon and Biogeochemistry Program and North American Carbon Program. https://doi.org/10.1575/1912/7777

Bourgeois, T., Orr, J. C., Resplandy, L., Terhaar, J., Ethé, C., Gehlen, M., et al. (2016). Coastal-ocean uptake of anthropogenic carbon. *Biogeosciences*, *13*, 4167–4185. https://doi.org/10.5194/bg-13-4167-2016

Broullón, D., Pérez, F. F., Velo, A., Hoppema, M., Olsen, A., Takahashi, T., et al. (2018). A global monthly climatology of total alkalinity: a neural network approach. *Earth System Science Data Discussions*, *2013*(August 2019), 1–31. https://doi.org/10.5194/essd-2018-111

Carter, B. R., Feely, R. A., Wanninkhof, R., Kouketsu, S., Sonnerup, R. E., Pardo, P. C., et al. (2019). Pacific Anthropogenic Carbon Between 1991 and 2017. *Global Biogeochemical Cycles*, *33*, 597–617. https://doi.org/10.1029/2018GB006154

Chan, F., Barth, J. A., Blanchette, C. A., Byrne, R. H., Chavez, F., Cheriton, O., et al. (2017). Persistent spatial structuring of coastal ocean acidification in the California Current System. *Scientific Reports*, *7*(1), 1–7. https://doi.org/10.1038/s41598-017-02777-y

Chau, T. T. T., Gehlen, M., & Chevallier, F. (2022). A seamless ensemble-based reconstruction of surface ocean pCO_2 and air-sea CO_2 fluxes over the global coastal and open oceans. *Biogeosciences*, *19*(4), 1087–1109. https://doi.org/10.5194/bg-19-1087-2022

Chavez, F. P., Takahashi, T., Cai, W. J., Friederich, G., Hales, B., Wanninkhof, R., & Feely, R. A. (2007). Coastal oceans. In *The First State of the Carbon Cycle Report (SOCCR): The North American Carbon Budget and Implications for the Global Carbon Cycle* (pp. 157–166). Washington, DC: US Climate Change Science Program.

Chen, C.-T. A., & Borges, A. V. (2009). Reconciling opposing views on carbon cycling in the coastal ocean: Continental shelves as sinks and near-shore ecosystems as sources of atmospheric CO_2. *Deep-Sea Research Part II: Topical Studies in Oceanography*, *56*(8–10), 578–590. https://doi.org/10.1016/j.dsr2.2008.12.009

Chen, S., Hu, C., Byrne, R. H., Robbins, L. L., & Yang, B. (2016). Remote estimation of surface pCO_2 on the West Florida Shelf. *Continental Shelf Research*, *128*(December 2015), 10–25. https://doi.org/10.1016/j.csr.2016.09.004

Christensen, J. P. (1994). Carbon export from continental shelves, denitrification and atmospheric carbon dioxide. *Continental Shelf Research*, *14*(5), 547–576. https://doi.org/10.1016/0278-4343(94)90103-1

Clement, D., & Gruber, N. (2018). The eMLR (C *) Method to Determine Decadal Changes in the Global Ocean Storage of Anthropogenic CO_2, 654–679. https://doi.org/10.1002/2017GB005819

Côté, J., Gravel, S., Méthot, A., Patoine, A., Roch, M., & Staniforth, A. (1998). The Operational CMC–MRB Global Environmental Multiscale (GEM) Model. Part I: Design Considerations and Formulation. *Monthly Weather Review*, *126*(6), 1373–1395. https://doi.org/10.1175/1520-0493(1998)126<1373:TOCMGE>2.0.CO;2

Coyle, K. O., Cheng, W., Hinckley, S. L., Lessard, E. J., Whitledge, T., Hermann, A. J., & Hedstrom, K. (2012). Model and field observations of effects of circulation on the timing and magnitude of nitrate utilization and production on the northern Gulf of Alaska shelf. *Progress in Oceanography*, *103*, 16–41. https://doi.org/10.1016/j.pocean.2012.03.002

Crawford, W. R., & Whitney, F. A. (1999). Mesoscale eddy aswirl with data in Gulf of Alaska. *Eos*, *80*(33), 365–370. https://doi.org/10.1029/EO080i033p00365-01

Crawford, W. R., Brickley, P. J., & Thomas, A. C. (2007). Mesoscale eddies dominate surface phytoplankton in northern Gulf of Alaska. *Progress in Oceanography*, *75*(2), 287–303. https://doi.org/10.1016/j.pocean.2007.08.016

Dai, M. (2021). What are the exchanges of carbon between the land-ocean-ice continuum? In *Integrated ocean carbon research: a summary of ocean carbon research, and vision of coordinated ocean carbon research and observations for the next decade* (R. Wanninkhof, C. Sabine, S. Aricò, p. 20). Paris, France: Intergovernmental Oceanographic Commission. Retrieved from https://unesdoc.unesco.org/ark:/48223/pf0000376708.locale=en

Dai, M., Su, J., Zhao, Y., Hofmann, E. E., Cao, Z., Cai, W., et al. (2022). Carbon Fluxes in the Coastal Ocean: Synthesis, Boundary Processes, and Future Trends. *Annual Review of Earth and Planetary Sciences*, *50*, 593–626. https://doi.org/10.1146/annurev-earth-032320- 090746

Dickson, A. G., Sabine, C. L., & Christian, J. R. (2007). *Guide to Best Practices for Ocean CO2 Measurements. PICES Spec. Publ.* (Vol. 3).

Dong, Y., Bakker, D. C. E., Bell, T. G., Huang, B., Landschützer, P., Liss, P. S., & Yang, M. (2022). Update on the Temperature Corrections of Global Air-Sea CO2 Flux Estimates. *Global Biogeochemical Cycles*, *36*(9). https://doi.org/10.1029/2022GB007360

Dorman, C. E., & Winant, C. D. (1995). Buoy observations of the atmosphere along the west coast of the United States, 1981-1990. *Journal of Geophysical Research*, *100*, 16029–16044.

Duke, P. J., Hamme, R. C., Ianson, D., Landschützer, P., Ahmed, M. M. M., Swart, N. C., & Covert, P. A. (2023a). ANN-NEP: A monthly surface pCO2 product for the Northeast Pacific open ocean from 1998-01-01 to 2019-12-31 (NCEI Accession 0277836) [Data set]. gov.noaa.nodc:0277836: NOAA National Centers for Environmental Information. https://doi.org/10.25921/c1w8-6v02

Duke, P. J., Richaud, B., Arruda, R., Länger, J., Schuler, K., Gooya, P., et al. (2023). Canada's marine carbon sink: an early career perspective on the state of research and existing knowledge gaps. *Facets*, *8*, 1–21. https://doi.org/10.1139/facets-2022-0214

Duke, P. J., Hamme, R. C., Ianson, D., Landschützer, P., Ahmed, M. M. M., Swart, N. C., & Covert, P. A. (2023b). Estimating marine carbon uptake in the northeast Pacific using a neural network approach. *Biogeosciences*, *20*(18), 3919–3941. https://doi.org/10.5194/bg-20-3919-2023

Duke, P. J., Hamme, R. C., Ianson, D., Landschützer, P., Swart, N. C., & Covert, P. A. (2024). ANN-NEPc: A monthly surface pCO2 product for the Northeast Pacific coastal ocean from 1998-01-01 to 2019-12-31 [Data set]. NOAA National Centers for Environmental Information (NCEI).

Durand, F., Piecuch, C. G., Becker, M., Papa, F., Raju, S. V., Khan, J. U., & Ponte, R. M. (2019). Impact of Continental Freshwater Runoff on Coastal Sea Level. *Surveys in Geophysics*, *40*(6), 1437–1466. https://doi.org/10.1007/s10712-019-09536-w

Evans, W., & Mathis, J. T. (2013). The Gulf of Alaska coastal ocean as an atmospheric CO2 sink. *Continental Shelf Research*, *65*, 52–63. https://doi.org/10.1016/j.csr.2013.06.013

Evans, W., Hales, B., & Strutton, P. G. (2011). Seasonal cycle of surface ocean p CO_2 on the Oregon shelf. *Journal of Geophysical Research*, *116*(C5), C05012. https://doi.org/10.1029/2010JC006625

Evans, W., Hales, B., Strutton, P. G., & Ianson, D. (2012). Sea-air CO 2 fluxes in the western Canadian coastal ocean. *Progress in Oceanography*, *101*(1), 78–91. https://doi.org/10.1016/j.pocean.2012.01.003

Evans, W., Hales, B., Strutton, P. G., Shearman, R. K., & Barth, J. A. (2015). Failure to bloom: Intense upwelling results in negligible phytoplankton response and prolonged CO2 outgassing over the Oregon shelf. *Journal of Geophysical Research: Oceans*, *120*(3), 1446–1461. https://doi.org/10.1002/2014JC010580

Evans, W., Pocock, K., Hare, A., Weekes, C., Hales, B., Jackson, J., et al. (2019). Marine CO2 patterns in the Northern Salish Sea. *Frontiers in Marine Science*, *5*(JAN), 1–18. https://doi.org/10.3389/fmars.2018.00536

Evans, W., Lebon, G. T., Harrington, C. D., Takeshita, Y., Bidlack, A., & Bay, H. (2022). Marine CO2 system variability along the northeast Pacific Inside Passage determined from an Alaskan ferry. *Biogeosciences*, *19*, 1277–1301. https://doi.org/10.5194/bg-19-1277-2022

Fassbender, A. J., Alin, S. R., Feely, R. A., Sutton, A. J., Newton, J. A., Krembs, C., et al. (2018). Seasonal carbonate chemistry variability in marine surface waters of the US Pacific Northwest. *Earth System Science Data*, *10*(3), 1367–1401. https://doi.org/10.5194/essd-10-1367-2018

Feely, R. A., Sabine, C. L., Hernandez-Ayon, J. M., Ianson, D., & Hales, B. (2008). Evidence for upwelling of corrosive “acidified” water onto the continental shelf. *Science*, *320*(5882), 1490–1492. https://doi.org/10.1126/science.1155676

Fennel, K., Alin, S., Barbero, L., Evans, W., Bourgeois, T., Cooley, S., et al. (2019). Carbon Cycling in the North American Coastal Ocean: A Synthesis. *Biogeosciences*, *16*, 1281–1304. https://doi.org/10.5194/bg-16-1281-2019

Fiechter, J., & Moore, A. M. (2009). Interannual spring bloom variability and Ekman pumping in the coastal Gulf of Alaska. *Journal of Geophysical Research: Oceans*, *114*(C6). https://doi.org/10.1029/2008JC005140

Ford, D. J., Tilstone, G. H., Shutler, J. D., Kitidis, V., Lobanova, P., Schwarz, J., et al. (2021). Wind speed and mesoscale features drive net autotrophy in the South Atlantic Ocean. *Remote Sensing of Environment*, *260*(July 2020), 112435. https://doi.org/10.1016/j.rse.2021.112435

Ford, D. J., Tilstone, G. H., Shutler, J. D., & Kitidis, V. (2022). Derivation of seawater p CO 2 from net community production identifies the South Atlantic Ocean as a CO 2 source. *Biogeosciences*, *19*, 93–115. https://doi.org/10.5194/bg-19-93-2022

Fourrier, M., Coppola, L., Claustre, H., D’Ortenzio, F., Sauzède, R., & Gattuso, J. P. (2020). A Regional Neural Network Approach to Estimate Water-Column Nutrient Concentrations and Carbonate System Variables in the Mediterranean Sea: CANYON-MED. *Frontiers in Marine Science*, *7*(August), 1–20. https://doi.org/10.3389/fmars.2020.00620

Franco, A. C., Ianson, D., Ross, T., Hamme, R. C., Monahan, A. H., Christian, J. R., et al. (2021). Anthropogenic and climatic contributions to observed carbon system trends in the Northeast Pacific. *Global Biogeochemical Cycles*, (Dic), 1–21. https://doi.org/10.1029/2020gb006829

Friedlingstein, P., O’Sullivan, M., Jones, M. W., Andrew, R. M., Bakker, D. C. E., Hauck, J., et al. (2023). Global Carbon Budget 2023. *Earth System Science Data*, *15*(12), 5301–5369. https://doi.org/10.5194/essd-15-5301-2023

Gargett, A. E. (1991). Physical processes and the maintenance of nutrient-rich euphotic zones. *Limnology and Oceanography*, *36*(8), 1527–1545. https://doi.org/10.4319/lo.1991.36.8.1527

Gasset, N., Fortin, V., Dimitrijevic, M., Carrera, M., Bilodeau, B., Muncaster, R., et al. (2021). A 10 km North American precipitation and land-surface reanalysis based on the GEM atmospheric model. *Hydrology and Earth System Sciences*, *25*(9), 4917–4945. https://doi.org/10.5194/hess-25-4917-2021

Global Monitoring and Forecasting Center GLORYS12V1. (2020). Global Ocean Physical Reanalysis Product, E.U. Copernicus Marine Service Information GLOBAL_REANALYSIS_PHY_001_030. https://doi.org/10.48670/moi-00021

Goddijn-Murphy, L. M., Woolf, D. K., Land, P. E., Shutler, J. D., & Donlon, C. (2015). The OceanFlux Greenhouse Gases methodology for deriving a sea surface climatology of CO2 fugacity in support of air-sea gas flux studies. *Ocean Science*, *11*(4), 519–541. https://doi.org/10.5194/os-11-519-2015

Good, S. A., Embury, O., Bulgin, C. E., & Mittaz, J. (2019). ESA Sea Surface Temperature Climate Change Initiative (SST_cci): Level 4 Analysis Climate Data Record, version 2.1. https://doi.org/10.5285/62c0f97b1eac4e0197a674870afe1ee6

Gooya, P., Swart, N. C., & Hamme, R. C. (2023). Time-varying changes and uncertainties in the CMIP6 ocean carbon sink from global to local scale. *Earth System Dynamics*, *14*(2), 383–398. https://doi.org/10.5194/esd-14-383-2023

Gruber, N., Clement, D., Carter, B. R., Feely, R. A., van Heuven, S., Hoppema, M., et al. (2019). The oceanic sink for anthropogenic CO2 from 1994 to 2007. *Science*, *363*(6432), 1193–1199. https://doi.org/10.1126/science.aau5153

Hales, B., Takahashi, T., & Bandstra, L. (2005). Atmospheric CO2 uptake by a coastal upwelling system. *Global Biogeochemical Cycles*, *19*(1). https://doi.org/10.1029/2004GB002295

Hales, B., Strutton, P. G., Saraceno, M., Letelier, R., Takahashi, T., Feely, R., et al. (2012). Satellite-based prediction of pCO 2 in coastal waters of the eastern North Pacific. *Progress in Oceanography*, *103*, 1–15. https://doi.org/10.1016/j.pocean.2012.03.001

Hauri, C., Schultz, C., Hedstrom, K., Danielson, S., Irving, B., C. Doney, S., et al. (2020). A regional hindcast model simulating ecosystem dynamics, inorganic carbon chemistry, and ocean acidification in the Gulf of Alaska. *Biogeosciences*, *17*(14), 3837–3857. https://doi.org/10.5194/bg-17-3837-2020

Hauri, C., Pagès, R., McDonnell, A. M. P., Stuecker, M. F., Danielson, S. L., Hedstrom, K., et al. (2021). Modulation of ocean acidification by decadal climate variability in the Gulf of Alaska. *Communications Earth & Environment*, *2*(1), 1–7. https://doi.org/10.1038/s43247-021-00254-z

Hermann, A. J., Hinckley, S., Dobbins, E. L., Haidvogel, D. B., Bond, N. A., Mordy, C., et al. (2009). Quantifying cross-shelf and vertical nutrient flux in the Coastal Gulf of Alaska with a spatially nested, coupled biophysical model. *Deep Sea Research Part II: Topical Studies in Oceanography*, *56*(24), 2474–2486. https://doi.org/10.1016/j.dsr2.2009.02.008

Hsieh, W. W., Ware, D. A., & Thornson, R. E. (1995). Wind-induced upwelling along the west coast of North America, 1899-1988. *Canadian Journal of Fisheries and Aquatic Sciences*, *52*(2), 325–334.

Ianson, D., & Allen, S. E. (2002). A two-dimensional nitrogen and carbon flux model in a coastal upwelling region. *Global Biogeochemical Cycles*, *16*(1).

Ianson, D., Allen, S. E., Harris, S. L., Orians, K. J., Varela, D. E., & Wong, C. S. (2003). The inorganic carbon system in the coastal upwelling region west of Vancouver Island, Canada. *Deep-Sea Research Part I: Oceanographic Research Papers*, *50*(8), 1023–1042. https://doi.org/10.1016/S0967-0637(03)00114-6

Ianson, D., Feely, R. A., Sabine, C. L., & Juranek, L. W. (2009). Features of coastal upwelling regions that determine net air-sea CO 2 flux. *Journal of Oceanography*, *65*(5), 677–687. https://doi.org/10.1007/s10872-009-0059-z

Ianson, D., Allen, S. E., Moore-Maley, B. L., Johannessen, S. C., & Macdonald, R. W. (2016). Vulnerability of a semienclosed estuarine sea to ocean acidification in contrast with hypoxia. *Geophysical Research Letters*, *43*(11), 5793–5801. https://doi.org/10.1002/2016GL068996

Jarníková, T., Olson, E. M., Allen, S. E., Ianson, D., & Suchy, K. D. (2022). A clustering approach to determine biophysical provinces and physical drivers of productivity dynamics in a complex coastal sea. *Ocean Science*, *18*(5), 1451–1475. https://doi.org/10.5194/os-18-1451-2022

Jarníková, T., Ianson, D., Allen, S. E., Shao, A., & Olson, E. M. (2022). Anthropogenic carbon increase has caused critical shifts in aragonite saturation across a sensitive coastal system. *Global Biogeochemical Cycles*. https://doi.org/10.1029/2021GB007024

Jean-Michel, L., Eric, G., Romain, B.-B., Gilles, G., Angélique, M., Marie, D., et al. (2021). The Copernicus Global 1 / 12 ° Oceanic and Sea Ice GLORYS12 Reanalysis. *Frontiers in Earth Science*, *9*(698876), 1–27. https://doi.org/10.3389/feart.2021.698876

Jones, S. D., Le Quéré, C., & Rdenbeck, C. (2012). Autocorrelation characteristics of surface ocean pCO2 and air-sea CO2 fluxes. *Global Biogeochemical Cycles*, *26*(2), 1–12. https://doi.org/10.1029/2010GB004017

Kalnay, E., Kanamitsu, M., Kistler, R., Collins, W., Deaven, D., Gandin, L., et al. (1996). The NCEP/NCAR 40-Year Reanalysis Project. *Bulletin of the American Meteorological Society*, *77*(3), 437–472. https://doi.org/10.1175/1520-0477(1996)077<0437:TNYRP>2.0.CO;2

Körtzinger, A. (1999). Determination of carbon dioxide partial pressure (pCO2). In *Methods of Seawater Analysis* (pp. 149–158). Verlag Chemie.

Landschützer, P., Gruber, N., Bakker, D. C. E., Schuster, U., Nakaoka, S., Payne, M. R., et al. (2013). A neural network-based estimate of the seasonal to inter-annual variability of the Atlantic Ocean carbon sink. *Biogeosciences*, *10*(11), 7793–7815. https://doi.org/10.5194/bg-10-7793-2013

Landschützer, P., Gruber, N., D.C.E.Bakker, & Schuster, U. (2014). Recent variability of the global ocean carbon sink. *Global Biogeochemical Cycles*, *28*(9), 927–949. https://doi.org/10.1002/2014GB004853

Landschützer, P., Gruber, N., Bakker, D. C. E., Stemmler, I., & Six, K. D. (2018). Strengthening seasonal marine CO2 variations due to increasing atmospheric CO2. *Nature Climate Change*, *8*(2), 146–150. https://doi.org/10.1038/s41558-017-0057-x

Landschützer, P., Laruelle, G. G., Roobaert, A., & Regnier, P. (2020). A uniform pCO2 climatology combining open and coastal oceans. *Earth System Science Data*, *12*(4), 2537–2553. https://doi.org/10.5194/essd-12-2537-2020

Landschützer, P., Gruber, N., & Bakker, D. C. E. (2020). An observation-based global monthly gridded sea surface pCO2 and air-sea CO2 flux product from 1982 onward and its monthly climatology. *NCEI Accession*. NOAA National Centers for Environmental Information. https://doi.org/10.7289/v5z899n6

Laruelle, G. G., Lauerwald, R., Pfeil, B., & Regnier, P. (2014). Regionalized global budget of the CO2 exchange at the air-water interface in continental shelf seas. *Global Biogeochemical Cycles*, *28*, 1199–1214. https://doi.org/10.1002/2014GB004832.Received

Laruelle, G. G., Landschützer, P., Gruber, N., Tison, J.-L., Delille, B., & Regnier, P. (2017). Global high-resolution monthly pCO2 climatology for the coastal ocean derived from neural network interpolation. *Biogeosciences Discussions*, (2014), 1–40. https://doi.org/10.5194/bg-2017-64

Laruelle, G. G., Cai, W.-J., Hu, X., Gruber, N., Mackenzie, F. T., & Regnier, P. (2018). Continental shelves as a variable but increasing global sink for atmospheric carbon dioxide. *Nature Communications*, *9*(454), 1–11. https://doi.org/10.1038/s41467-017-02738-z

Legge, O., Johnson, M., Hicks, N., Jickells, T., Diesing, M., Aldridge, J., et al. (2020). Carbon on the Northwest European Shelf: Contemporary Budget and Future Influences. *Frontiers in Marine Science*, *7*(March). https://doi.org/10.3389/fmars.2020.00143

Li, X., Bellerby, R., Ge, J., Wallhead, P., Liu, J., & Yang, A. (2019). Retrieving monthly and interannual total-scale pH on the East China Sea shelf using an artificial neural network: ANN-pH-v1. *Geoscientific Model Development Discussions*, 1–15. https://doi.org/10.5194/gmd-2019-236

Li, X., Bellerby, R. G. J., Wallhead, P., Ge, J., Liu, J., Liu, J., & Yang, A. (2020). A Neural Network-Based Analysis of the Seasonal Variability of Surface Total Alkalinity on the East China Sea Shelf. *Frontiers in Marine Science*, *7*(April). https://doi.org/10.3389/fmars.2020.00219

Linares-Rodriguez, A., Ruiz-Arias, J. A., Pozo-Vazquez, D., & Tovar-Pescador, J. (2013). An artificial neural network ensemble model for estimating global solar radiation from Meteosat satellite images. *Energy*, *61*, 636–645. https://doi.org/10.1016/j.energy.2013.09.008

Liu, K.-K., Atkinson, L., Quinones, R., & Talaue-McManus, L. (2010). Carbon and Nutrient Fluxes in Continental Margins. *Global Change – The IGBP Series*. Springer-Verlag Berlin Heidelberg.

Mackenzie, F. T., Lerman, A., & Ver, L. M. B. (1998). Role of the continental margin in the global carbon balance during the past three centuries. *Geology*, *26*(5), 423–426. https://doi.org/10.1130/0091-7613(1998)026<0423:ROTCMI>2.3.CO;2

Marchese, C., Hunt, B. P. V., Giannini, F., Ehrler, M., & Costa, M. (2022). Bioregionalization of the coastal and open oceans of British Columbia and Southeast Alaska based on Sentinel-3A satellite-derived phytoplankton seasonality. *Frontiers in Marine Science*, *9*(September), 1–22. https://doi.org/10.3389/fmars.2022.968470

McKinley, G. A., Pilcher, D. J., Fay, A. R., Lindsay, K., Long, M. C., & Lovenduski, N. S. (2016). Timescales for detection of trends in the ocean carbon sink. *Nature*, *530*(7591), 469–472. https://doi.org/10.1038/nature16958

Merchant, C. J., Embury, O., Bulgin, C. E., Block, T., Corlett, G. K., Fiedler, E., et al. (2019). Satellite-based time-series of sea-surface temperature since 1981 for climate applications. *Scientific Data*, *6*(1), 1–18. https://doi.org/10.1038/s41597-019-0236-x

Messié, M., & Chavez, F. P. (2015). Seasonal regulation of primary production in eastern boundary upwelling systems. *Progress in Oceanography*, *134*, 1–18. https://doi.org/10.1016/j.pocean.2014.10.011

Murphy, P. P., Nojiri, Y., Harrison, D. E., & Larkin, N. K. (2001). Scales of spatial variability for surface ocean pCO2 in the Gulf of Alaska and Bering Sea: Toward a sampling strategy. *Geophysical Research Letters*, *28*(6), 1047–1050. https://doi.org/10.1029/2000GL012375

Nemcek, N., Ianson, D., & Tortell, P. D. (2008). A high-resolution survey of DMS, CO2, and O2/Ar distributions in productive coastal waters. *Global Biogeochemical Cycles*, *22*(2), 1–13. https://doi.org/10.1029/2006GB002879

O'Carroll, A. G., Armstrong, E. M., Beggs, H. M., Bouali, M., Casey, K. S., Corlett, G. K., et al. (2019). Observational Needs of Sea Surface Temperature. *Frontiers in Marine Science*, *6*. Retrieved from https://www.frontiersin.org/articles/10.3389/fmars.2019.00420

de Oña, J., & Garrido, C. (2014). Extracting the contribution of independent variables in neural network models: A new approach to handle instability. *Neural Computing and Applications*, *25*(3–4), 859–869. https://doi.org/10.1007/s00521-014-1573-5

Parard, G., Charantonis, A. A., & Rutgerson, A. (2015). Remote sensing the sea surface CO2 of the Baltic Sea using the SOMLO methodology. *Biogeosciences*, *12*(11), 3369–3384. https://doi.org/10.5194/bg-12-3369-2015

Parard, Gaëlle, Charantonis, A. A., & Rutgersson, A. (2016). Using satellite data to estimate partial pressure of CO2 in the Baltic Sea. *Journal of Geophysical Research G: Biogeosciences*, *121*(3), 1002–1015. https://doi.org/10.1002/2015JG003064

Pilcher, D. J., Siedlecki, S. A., Hermann, A. J., Coyle, K. O., Mathis, J. T., & Evans, W. (2018). Simulated Impact of Glacial Runoff on CO2 Uptake in the Gulf of Alaska. *Geophysical Research Letters*, *45*(2), 880–890. https://doi.org/10.1002/2017GL075910

Reed, R. K., & Schumacher, J. D. (1986). Current Measurements along the Shelf Break in the Gulf of Alaska. *Journal of Physical Oceanography*, *16*(11), 1985–1990. https://doi.org/10.1175/1520-0485(1986)016<1985:CMATSB>2.0.CO;2

Regnier, P., Resplandy, L., Najjar, R. G., & Ciais, P. (2022). The land-to-ocean loops of the global carbon cycle. *Nature*, *603*(7901), 401–410. https://doi.org/10.1038/s41586-021-04339-9

Resplandy, L., Séférian, R., & Bopp, L. (2015). Natural variability of CO2 and O2 fluxes: What can we learn from centuries-long climate models simulations? *Journal of Geophysical Research: Oceans*, *120*(1), 384–404. https://doi.org/10.1002/2014JC010463

Resplandy, L., Hogikyan, A., Müller, J. D., Najjar, R. G., Bange, H. W., Bianchi, D., et al. (2024). A Synthesis of Global Coastal Ocean Greenhouse Gas Fluxes. *Global Biogeochemical Cycles*, *38*(1), e2023GB007803. https://doi.org/10.1029/2023GB007803

Revelle, R., & Suess, H. E. (1957). Carbon Dioxide Exchange Between Atmosphere and Ocean and the Question of an Increase of Atmospheric CO2 during the Past Decades. *Tellus*, *9*(1), 18–27. https://doi.org/10.3402/tellusa.v9i1.9075

Reynolds, R. W., Rayner, N. A., Smith, T. M., Stokes, D. C., & Wang, W. (2002). An Improved In Situ and Satellite SST Analysis for Climate. *Journal of Climate*, *15*(13), 1609–1625. https://doi.org/10.1175/1520-0442(2002)015<1609:AIISAS>2.0.CO;2

Ribalet, F., Marchetti, A., Hubbard, K. A., Brown, K., Durkin, C. A., Morales, R., et al. (2010). Unveiling a phytoplankton hotspot at a narrow boundary between coastal and offshore waters. *Proceedings of the National Academy of Sciences of the United States of America*, *107*(38), 16571–16576. https://doi.org/10.1073/pnas.1005638107

Roobaert, A., Laruelle, G. G., Landschützer, P., Gruber, N., Chou, L., & Regnier, P. (2019). The Spatiotemporal Dynamics of the Sources and Sinks of CO2 in the Global Coastal Ocean. *Global Biogeochemical Cycles*, *33*(12), 1693–1714. https://doi.org/10.1029/2019GB006239

Roobaert, A., Regnier, P., Landschützer, P., & Laruelle, G. G. (2024). A novel sea surface pCO_2-product for the global coastal ocean resolving trends over 1982–2020. *Earth System Science Data*, *16*(1), 421–441. https://doi.org/10.5194/essd-16-421-2024

Sabine, C. L., Feely, R. A., Gruber, N., Key, R. M., Lee, K., Bullister, J. L., et al. (2004). The Oceanic Sink for Anthropogenic CO 2. *Science*, *305*(July), 367–372. https://doi.org/10.1126/science.1097403

Sarmiento, J. L., & Gruber, N. (2006). *Ocean Biogeochemical Dynamics*. Princeton: Princeton University Press.

Sathyendranath, S., Jackson, T., Brockmann, C., Brotas, V., Calton, B., Chuprin, A., et al. (2021). ESA Ocean Colour Climate Change Initiative (Ocean_Colour_cci): Global chlorophyll-a data products gridded on a geographic projection, Version 5.0. Retrieved from https://catalogue.ceda.ac.uk/uuid/e9f82908fd9c48138b31e5cfaa6d692b

Sharkey, A. J. C. (1999). *Combining Artificial Neural Nets: Ensemble and Modular Multi-Net Systems*. Berlin: Springer.

Sharp, J. D., Fassbender, A. J., Carter, B. R., Lavin, P. D., & Sutton, A. J. (2022). A monthly surface pCO2product for the California Current Large Marine Ecosystem. *Earth System Science Data*, *14*(4), 2081–2108. https://doi.org/10.5194/essd-14-2081-2022

Shutler, J. D., Land, P. E., Piolle, J. F., Woolf, D. K., Goddijn-Murphy, L., Paul, F., et al. (2016). FluxEngine: A flexible processing system for calculating atmosphere-ocean carbon dioxide gas fluxes and climatologies. *Journal of Atmospheric and Oceanic Technology*, *33*(4), 741–756. https://doi.org/10.1175/JTECH-D-14-00204.1

Siedlecki, S. A., Pilcher, D. J., Hermann, A. J., Coyle, K., & Mathis, J. (2017). The Importance of Freshwater to Spatial Variability of Aragonite Saturation State in the Gulf of Alaska. *Journal of Geophysical Research: Oceans*, *122*(11), 8482–8502. https://doi.org/10.1002/2017JC012791

Simpson, E., Ianson, D., & Kohfeld, K. E. (2022). Using End-Member Models to Estimate Seasonal Carbonate Chemistry and Acidification Sensitivity in Temperate Estuaries. *Geophysical Research Letters*, *49*(2), e2021GL095579. https://doi.org/10.1029/2021GL095579

Stabeno, P. J., Bond, N. A., Hermann, A. J., Kachel, N. B., Mordy, C. W., & Overland, J. E. (2004). *Meteorology and oceanography of the Northern Gulf of Alaska*. *Continental Shelf Research* (Vol. 24). https://doi.org/10.1016/j.csr.2004.02.007

Sun, H., He, J., Chen, Y., & Zhao, B. (2021). Space-Time Sea Surface pCO2 Estimation in the North Atlantic Based on CatBoost. *Remote Sensing*, *13*(14), 2805. https://doi.org/10.3390/rs13142805

Sutton, A. J., Wanninkhof, R., Sabine, C. L., Feely, R. A., Cronin, M. F., & Weller, R. A. (2017). Variability and trends in surface seawater pCO 2 and CO 2 flux in the Pacific Ocean. *Geophysical Research Letters*, *44*(11), 5627–5636. https://doi.org/10.1002/2017GL073814

Sutton, Adrienne J., Feely, R. A., Maenner-Jones, S., Musielwicz, S., Osborne, J., Dietrich, C., et al. (2019). Autonomous seawater pCO 2 and pH time series from 40 surface buoys and the emergence of anthropogenic trends. *Earth System Science Data*, *11*(1), 421–439. https://doi.org/10.5194/essd-11-421-2019

Takahashi, T., Olafsson, J., Goddard, J. G., Chipman, D. W., & Sutherland, S. C. (1993). Seasonal variation of CO2 and nutrients in the high-latitude surface oceans: A comparative study. *Global Biogeochemical Cycles*, *7*(4), 843–878. https://doi.org/10.1029/93GB02263

Takahashi, T., Sutherland, S. C., Sweeney, C., Poisson, A., Metzl, N., Tilbrook, B., et al. (2002). Global sea-air CO2 flux based on climatological surface ocean pCO2, and seasonal biological and temperature effects. *Deep-Sea Research Part II: Topical Studies in Oceanography*, *49*(9–10), 1601–1622. https://doi.org/10.1016/S0967-0645(02)00003-6

Takahashi, T., Sutherland, S. C., Feely, R. A., & Wanninkhof, R. (2006). Decadal change of the surface water pCO_2 in the North Pacific: A synthesis of 35 years of observations. *Journal of Geophysical Research*, *111*(C7), C07S05. https://doi.org/10.1029/2005JC003074

Talley, L. D. (1985). Ventilation of the Subtropical North Pacific: The Shallow Salinity Minimum. *Journal of Physical Oceanography*, *15*(6), 633–649. https://doi.org/10.1175/1520-0485(1985)015<0633:VOTSNP>2.0.CO;2

Teeter, L., Hamme, R. C., Ianson, D., & Bianucci, L. (2018). Accurate Estimation of Net Community Production From O2/Ar Measurements. *Global Biogeochemical Cycles*, *32*(8), 1163–1181. https://doi.org/10.1029/2017GB005874

Thomson, R. E. (1981). *Oceanography of the British Columbia Coast*. *Canadian special publications of fisheries and aquatic sciences* (Vol. 56).

Thomson, R. E., & Ware, D. M. (1996). A current velocity index of ocean variability. *Journal of Geophysical Research: Oceans*, *101*(C6), 14297–14310. https://doi.org/10.1029/96JC01055

Tortell, P. D., Merzouk, A., Ianson, D., Pawlowicz, R., & Yelland, D. R. (2012). Influence of regional climate forcing on surface water pCO_2,ΔO_2/Ar and dimethylsulfide (DMS) along the southern British Columbia coast. *Continental Shelf Research*, *47*, 119–132. https://doi.org/10.1016/j.csr.2012.07.007

Verra. (2023). *Verified Carbon Standard Program Guide v4.5*. Verra. Retrieved from https://verra.org/programs/verified-carbon-standard/vcs-version-4-rules-and-requirements/

Wang, H., Hu, X., Cai, W.-J., & Sterba-Boatwright, B. (2017). Decadal fCO_2 trends in global ocean margins and adjacent boundary current-influenced areas. *Geophysical Research Letters*, *44*(17), 8962–8970. https://doi.org/10.1002/2017GL074724

Wanninkhof, R. (2014). Relationship between wind speed and gas exchange over the ocean revisited. *Limnology and Oceanography: Methods*, *12*, 351–362. https://doi.org/10.4319/lom.2014.12.351

Ward, N. D., Megonigal, J. P., Bond-Lamberty, B., Bailey, V. L., Butman, D., Canuel, E. A., et al. (2020). Representing the function and sensitivity of coastal interfaces in Earth system models. *Nature Communications*, *11*(1), 2458. https://doi.org/10.1038/s41467-020-16236-2

Ware, D. M., & Thomson, R. E. (2005). Bottom-Up Ecosystem Trophic Dynamics Determine Fish Production in the Northeast Pacific. *Science*, *308*(5726), 1280–1284. https://doi.org/10.1126/science.1109049

Watson, A. J., Schuster, U., Shutler, J. D., Holding, T., Ashton, I. G. C., Landschützer, P., et al. (2020). Revised estimates of ocean-atmosphere CO_2 flux are consistent with ocean carbon inventory. *Nature Communications*, *11*(1), 1–6. https://doi.org/10.1038/s41467-020-18203-3

Weingartner, T. J., Coyle, K., Finney, B., Hopcroft, R., Whitledge, T., Brodeur, R., et al. (2002). The Northeast Pacific GLOBEC Program: Coastal Gulf of Alaska. *Oceanography*, *15*(2), 48–63. https://doi.org/10.5670/oceanog.2002.21

Weiss, R. F. (1974). Carbon dioxide in water and seawater: the solubility of a non-ideal gas. *Marine Chemistry*, *2*, 203–215. https://doi.org/10.1016/0304-4203(74)90015-2

Whitney, F., & Robert, M. (2002). Structure of Haida Eddies and their transport of nutrient from coastal margins into the NE pacific ocean. *Journal of Oceanography*, *58*(5), 715–723. https://doi.org/10.1023/A:1022850508403

Whitney, F. A., Crawford, W. R., & Harrison, P. J. (2005). Physical processes that enhance nutrient transport and primary productivity in the coastal and open ocean of the subarctic NE Pacific. *Deep-Sea Research Part II: Topical Studies in Oceanography*, *52*(5–6), 681–706. https://doi.org/10.1016/j.dsr2.2004.12.023

Wilkerson, F. P., & Dugdale, R. C. (1987). The use of large shipboard barrels and drifters to study the effects of coastal upwelling on phytoplankton dynamics1, 2. *Limnology and Oceanography*, *32*(2), 368–382. https://doi.org/10.4319/lo.1987.32.2.0368

Wong, C. S., Christian, J. R., Emmy Wong, S. K., Page, J., Xie, L., & Johannessen, S. (2010). Carbon dioxide in surface seawater of the eastern North Pacific Ocean (Line P), 1973-2005. *Deep-Sea Research Part I: Oceanographic Research Papers*, *57*(5), 687–695. https://doi.org/10.1016/j.dsr.2010.02.003

Woolf, D. K., Land, P. E., Shutler, J. D., Goddijn-Murphy, L. M., & Donlon, C. J. (2016). On the calculation of air-sea fluxes of CO2 in the presence of temperature and salinity gradients. *Journal of Geophysical Research: Oceans*, *121*(5), 3010–3028. https://doi.org/10.1002/2015JC011516

Xu, S., Park, K., Wang, Y., Chen, L., Qi, D., & Li, B. (2019). Variations in the summer oceanic pCO 2 and carbon sink in Prydz Bay using the self-organizing map analysis approach. *Biogeosciences*, *16*(3), 797–810. https://doi.org/10.5194/bg-16-797-2019

Yasunaka, S., Siswanto, E., Olsen, A., Hoppema, M., Watanabe, E., Fransson, A., et al. (2018). Arctic Ocean CO2 uptake: An improved multiyear estimate of the air-sea CO2 flux incorporating chlorophyll a concentrations. *Biogeosciences*, *15*(6), 1643–1661. https://doi.org/10.5194/bg-15-1643-2018